Spin transitions and compressibility of ε-Fe_7N_3 and γ'-Fe_4N: implications for iron alloys in terrestrial planet cores

Mingda Lv[1,*], Jiachao Liu[1,*,†], Feng Zhu[2,‡], Jie Li[2], Dongzhou Zhang[3,4], Yuming Xiao[5], Susannah M. Dorfman[1,*]

[1]Department of Earth and Environmental Sciences, Michigan State University, MI 48824, USA.

[2]Department of Earth and Environmental Sciences, University of Michigan, MI 48109, USA.

[3]Hawaii Institute of Geophysics and Planetology, University of Hawaii at Manoa, HI 96822, USA.

[4]GeoSoiEnviroCARS, University of Chicago, Argonne National Laboratory, Argonne, IL 60439, USA.

[5]High Pressure Collaborative Access Team (HPCAT), X-ray Science Division, Argonne National Laboratory, Argonne, IL 60439, USA.

[*] Corresponding author: Mingda Lv (lyumingd@msu.edu), Jiachao Liu (jiacliu@pku.edu.cn), Susannah M. Dorfman (dorfman3@msu.edu)

[†] Now at Key Laboratory of Orogenic Belts and Crustal Evolution, School of Earth and Space Sciences, Peking University, Beijing 100871, China.

[‡] Now at Hawaii Institute of Geophysics and Planetology, University of Hawaii at Manoa, HI 96822, USA.

Key Points:

- Spin transition in ε-Fe_7N_3 and γ'-Fe_4N at 300 K completes at 43 and 34 GPa, respectively
- The completion of spin transition leads to stiffening in bulk modulus of ε-Fe_7N_3, but not in γ'-Fe_4N
- Evidence for spin transitions in Fe-light-element alloys and their effects are re-examined

Abstract

Iron nitrides are possible constituents of the cores of Earth and other terrestrial planets. Pressure-induced magnetic changes in iron nitrides and effects on compressibility remain poorly understood. Here we report synchrotron X-ray emission spectroscopy (XES) and X-ray diffraction (XRD) results for ε-Fe_7N_3 and γ'-Fe_4N up to 60 GPa at 300 K. The XES spectra reveal completion of high- to low-spin transition in ε-Fe_7N_3 and γ'-Fe_4N at 43 and 34 GPa, respectively. The completion of the spin transition induces stiffening in bulk modulus of ε-Fe_7N_3 by 22% at ~40 GPa, but has no resolvable effect on the compression behavior of γ'-Fe_4N. Fitting pressure-volume data to the Birch-Murnaghan equation of state yields V_0 = 83.29±0.03 (Å^3), K_0 = 232±9 GPa, K_0' = 4.1±0.5 for nonmagnetic ε-Fe_7N_3 above the spin transition completion pressure, and V_0 = 54.82±0.02 (Å^3), K_0 = 152±2 GPa, K_0' = 4.0±0.1 for γ'-Fe_4N over the studied pressure range. By re-examining evidence for spin transition and effects on compressibility of other candidate components of terrestrial planet cores, Fe_3S, Fe_3P, Fe_7C_3, and Fe_3C based on previous XES and XRD measurements, we located the completion of high- to low-spin transition at ~67, 38, 50, and 30 GPa at 300 K, respectively. The completion of spin transitions of Fe_3S, Fe_3P and Fe_3C induces elastic stiffening, whereas that of Fe_7C_3 induces elastic softening. Changes in compressibility at completion of spin transitions in iron-light element alloys may influence the properties of Earth's and planetary cores.

1 Introduction

The Fe-Ni alloy that comprises the Earth's core must also contain light elements based on both geophysical observations (Birch, 1952) and compositions of planetary building blocks (Mcdonough & Sun, 1995), with potential implications for volatile storage and cycling within our planet. The leading candidate light elements for Earth's core include silicon, oxygen, sulfur, carbon, and hydrogen (Poirier, 1994); in addition to a possible mixture of these, nitrogen has been more recently proposed as a candidate light element in the core (e.g., Kusakabe et al., 2019; Minobe et al., 2015) based on structural stability and physical properties of iron nitrides (β-Fe_7N_3) extrapolated to core conditions. Additional support for the presence of iron nitrides in planetary interiors is provided by observations of iron nitrides in iron meteorites (Rubin & Ma, 2017) and in inclusions in superdeep diamonds, which potentially incorporate material from Earth's core-mantle boundary region (Kaminsky & Wirth, 2017) or locally reduced domains of Earth's mantle (Zedgenizov & Litasov, 2017). The behavior of nitrogen-bearing iron alloys and compounds at conditions relevant to both accretion and the modern core is thus important to evaluate the potential abundance of nitrogen in Earth's interior (e.g., Kusakabe et al., 2019; Litasov et al., 2017; Liu et al., 2019; Minobe et al., 2015). The few constraints on the identities and abundances of core light elements include observed seismological characteristics of Earth's inner and outer core, particularly ~4-7% density deficit of the core relative to properties of Fe-Ni noted since (Birch, 1952). Available constraints on thermoelasticity of solid iron nitrides from previous studies (e.g., Adler & Williams, 2005; Breton et al., 2019; Kusakabe et al., 2019; Litasov et al., 2017) can be extrapolated for comparison to Earth's core, but extrapolation depends on stability and electronic/magnetic properties of these materials under high pressure conditions which remain poorly understood.

A wide range of stable iron nitride compounds with varying stoichiometries are stabilized by different conditions (De Waele et al., 2019; Wriedt et al., 1987). Stable iron nitrides at 1 bar include nonstoichiometric ε-Fe_3N_x (0.75 < x < 1.4) with iron atoms arranged in a hexagonal-close-packed structure, and stoichiometric γ'-Fe_4N adopting a cubic-close-packed structure (Widenmeyer et al., 2014; Wriedt et al., 1987). Previous studies have identified additional structures in the Fe-N system stabilized by high pressure (e.g., De Waele et al., 2019; Wetzel et al., 2019; Widenmeyer et al., 2014). The ε-Fe_7N_3 structure (same stoichiometry as $Fe_3N_{x=1.3}$, space group $P6_322$) remains stable up to 51 GPa and 300 K (Adler & Williams, 2005), and was observed to transform to β-Fe_7N_3 above 41 GPa and ~1000 K (Minobe et al., 2015). γ'-Fe_4N (space group $Pm\overline{3}m$) is predicted to decompose to β-Fe_7N_3 + ε-Fe at ~56 GPa and 300 K based on thermodynamic analysis (Breton et al., 2019). At high temperatures, γ'-Fe_4N was observed to transform to ε-Fe_4N above 1373 K and 8.5 GPa (Guo et al., 2013), and decompose to Fe + β-Fe_7N_3 above 41 GPa at ~1000 K (Minobe et al., 2015). β-Fe_7N_3 was observed to remain stable up to 3100 K and 135 GPa, and proposed to exist in the Earth's solid inner core (Kusakabe et al., 2019). In addition, a new crystal structure of Fe_7N_3 with space group $C2/m$ was predicted to be stable under Earth's core conditions (Sagatov et al., 2019). However, due to the complex stoichiometries and structural variations in iron nitrides at high pressure and temperature conditions, understanding of high-pressure phase stability in this system remains incomplete.

The effects of incorporating nitrogen in iron alloys and compounds include not only modifying stable crystalline structure, but also the arrangement and bonding style of electrons in *d* orbitals around iron atoms that control magneto-elastic properties (e.g., Sifkovits et al., 1999; Widenmeyer et al., 2014). Electronic structure of iron nitrides have been investigated by first principles calculations and experimental measurements, which indicate that the chemical bonding in ε-Fe_7N_3 (e.g., Zhang et al., 2012) and γ-Fe_4N (e.g., dos Santos & Samudio Pérez, 2016) are complex mixtures of metallic, covalent, and ionic characters. Additionally, iron nitrides undergo pressure-induced magnetic transitions, which may affect thermodynamics and elasticities of Fe-N alloys and compounds at high pressures (e.g., dos Santos & Samudio Pérez, 2016; Ishimatsu et al., 2003; Popov et al., 2015). At 1 bar, the *d*-orbital electrons in Fe in all known Fe-N compounds adopt a high-spin ferromagnetic arrangement and are remarkable for high saturation of magnetism (which generally decreases with N concentration): the magnetic moment of ε-Fe_3N_x ranges from 2.0 to 0.2 μ_B per Fe atom as N concentration increases from x = 1 to 1.48 (Leineweber et al., 2001), while the magnetic moment of γ'-Fe_4N is 2.3 μ_B per Fe atom (Dirba et al., 2015). Only a few high-pressure studies on magnetism of the Fe-N system exist, and the magnetic transition pressures of iron nitrides and their effects on elasticities are largely unknown. Experiments on pressure-induced magnetic transitions of ε-Fe_3N_x have not been conducted. γ'-Fe_4N undergoes a ferromagnetic to paramagnetic transition at 24 GPa and 300 K as resolved by X-ray magnetic circular dichroism (XMCD) measurements (Ishimatsu et al., 2003), while first-principles calculations predicted the magnetic to nonmagnetic transition in γ'-Fe_4N occurs at 250 GPa (Popov et al., 2015). Systematic experimental constraints on pressure-induced magnetic transitions in both ε-Fe_3N_x and γ'-Fe_4N from ferromagnetic to paramagnetic or nonmagnetic state and the coupling between these electronic arrangements and elasticities and phase stability are necessary for an improved understanding of the physical properties of iron nitrides.

The identification of magneto-elastic coupling behavior in other iron alloy systems such as Fe-C, Fe-S, and Fe-P (recently reviewed by Caracas, 2016) provides additional motivation to test whether the Fe-N system behaves similarly. In the electronically- and structurally-similar Fe-C system, ferromagnetic (FM) Fe-C compounds undergo transitions first to a paramagnetic (PM) state, and then to a low-spin non-magnetic (NM) state, and these transitions have been proposed to significantly affect compressibility of Fe-C materials (e.g., Chen et al., 2012; Chen et al., 2018; Lin et al., 2004b; Mookherjee et al., 2011; Prescher et al., 2012). The pressure-induced magnetic transition of Fe-S (e.g., Chen et al., 2007; Lin et al., 2004a) and Fe-P compounds (e.g., Gu et al., 2014, 2016; Lai et al., 2020) have also been reported as well to affect compressibility and sound velocities. Due to the lack of characterization of electronic states at high pressures in previous studies of compression and phase transitions of iron nitrides (e.g., Adler & Williams, 2005; Breton et al., 2019; Litasov et al., 2017), the amount and role of N in Earth's core relative to other candidate light elements remains poorly constrained.

Magnetic transitions at high pressures have been experimentally detected using methods that directly characterize electronic states, as well as methods that indirectly assess magnetism through its effects on elasticity and compression behavior. The total spin moment of Fe, ranging from high to low spin, can be characterized by X-ray emission spectroscopy (XES). The appearance of the satellite emission peak $K_{\beta'}$ located at the lower energy relative to the main emission peak $K_{\beta 1,3}$ is a result of the 3*p*-3*d* core-hole exchange interaction in the final state of the emission process. That is, the intensity of the satellite peak depends on the spin polarization of the 3*d* shell and is sensitive to the net magnetic spin state. The collapse of the magnetization of Fe is characterized by the disappearance of the low-energy satellite due to the loss of 3*d* magnetic moment (e.g., Badro et al., 2003; Badro et al., 2004). Therefore, the local spin moment change of iron atoms revealed by XES can distinguish between high-spin (FM or PM) states vs. low-spin (NM) states. XES spectroscopy performed at high pressures using a synchrotron X-ray source has been used to study magnetic spin transitions in Fe-C, Fe-S, and Fe-P compounds (e.g., Chen et al., 2018; Chen et al., 2014; Gu et al., 2016; Lin et al., 2004b; Shen et al., 2003). Characterizing magneto-elastic coupling requires complementary information provided by spectroscopic methods such as X-ray emission and structural/elastic methods such as X-ray diffraction to confirm magnetic transitions and discontinuous compression behavior operate in tandem (e.g., Chen et al., 2014). However, no such study has been conducted in the Fe-N system.

Here we present a systematic study of magnetic transitions and compressibility of iron-nitrides, ε-Fe_7N_3 and γ'-Fe_4N, using synchrotron XES and XRD measurements up to 60 GPa at 300 K. Compression behavior of both compounds is monitored by dense pressure-volume (*P*-*V*) data coverage, combined with total spin moment indicated by XES, to determine any effects of magnetic transitions on the incompressibility of iron nitrides. Observed behavior is compared to the effect of magneto-elastic coupling in other Fe alloys studied using the same protocol.

2 Experimental methods

High purity nonstoichiometric ε-Fe_7N_3 and γ'-Fe_4N powders (99.9%, Kojundo Chemical Lab. Co. Ltd., average grain size ~1 μm) were used as starting materials. XRD for both samples at ambient conditions confirms unit cell volumes in good agreement with previous studies of ε-Fe_7N_3 (Adler & Williams, 2005; Kusakabe et al., 2019; Litasov et al., 2017; Minobe et al., 2015) and γ'-Fe_4N (Adler & Williams, 2005; Guo et al., 2013). For the nonstoichiometric ε-Fe_7N_3, the ambient volume measured for our sample V_0 = 86.32(±0.01) $Å^3$ is consistent with a linear relationship between unit-cell volume and nitrogen content in ε-Fe_3N_x, $V = 10.637x + 72.858$ (Litasov et al., 2017) when x is 1.27.

XES of ε-Fe_7N_3 and γ'-Fe_4N was measured up to 60 GPa at intervals of ~5 GPa. Compression in the diamond anvil cell (DAC) was performed using two pairs of diamond anvils with 200-μm flat culet. In each DAC, a flake of ε-Fe_7N_3 (~ 20 × 20 × 10 μm^3) or γ'-Fe_4N (~ 15 × 23 × 10 μm^3) sample was loaded in a 100-μm diameter sample chamber confined by a pre-indented Be gasket. The sample chamber was drilled in the center of the Be gasket with pre-indented thickness of ~30 μm using the laser drilling system at HPCAT (Sector 16) at the Advanced Photon Source (APS), Argonne National Laboratory (ANL) (Hrubiak et al., 2015). Silicone oil (Alfa Aesar) served as the pressure-transmitting medium and a 5-μm ruby ball was loaded into the sample chamber as the pressure standard. Pressures were determined by ruby fluorescence (Mao et al., 1986) before and after each XES collection, and differed by up to 10% due to relaxation of the sample or cell assembly. The XES measurements were performed at 300 K at beamline 16-ID-D of the APS, ANL. The incident X-ray beam was focused to 5×7 μm^2 full width at half maximum at the sample position. The fluorescence signal was observed through the Be gasket. The incident X-ray energy was 11.3 keV with a bandwidth of ~1 eV was used for the experiments. Fe K_β emission was selected by silicon analyzer and reflected to a silicon detector with an energy step of about 0.3 eV. Each spectrum was recorded for about 40 min and 3 spectra were taken to accumulate at least 30,000 counts at the Fe K_β main peak at each pressure. All spectra were normalized to area and aligned to the position of the Fe K_β main peak (Fig. 2). The high-spin reference is the sample spectrum at 1 bar, and low-spin references are the spectrum of FeS_2 at 1 bar collected using the same setup and the sample spectrum at 60 GPa. Intensity difference between the sample and references was integrated over the energy range of the satellite K_β' peak (7030-7053.0 eV) using the integrated relative difference method (Mao et al., 2014). Uncertainty in total spin moment was determined based on difference in calculations using FeS_2 vs. pressurized sample as low-spin references.

XRD measurements were carried out at 300 K up to 60 GPa with 1-2 GPa steps. The sample flakes of ε-Fe_7N_3 (~ 20 × 20 × 10 μm^3) and γ'-Fe_4N (~ 15 × 23 × 10 μm^3) were loaded side-by-side in the sample chamber of a DAC with a pair of 300-μm-culet diamonds. The sample chamber was drilled in the center of the Re gasket with a pre-indented thickness of ~30 μm using the laser drilling system at HPCAT (Hrubiak et al., 2015). Au powder (>99.95%, Goodfellow) was spread on top of the samples to serve as the pressure calibrant (Fei et al., 2007). Because the Au (111) peak overlapped with of ε-Fe_7N_3 (110) peak, we use the pressure calculated from Au at the position of the γ'-Fe_4N sample to represent the pressure at all sample positions. A flake of pure Fe (>99.997%, Alfa Aesar) with a size of ~ 25 × 23 × 10 μm^3 was loaded alongside the samples as a secondary reference to monitor the hydrostaticity of stress conditions in the sample chamber (Liu et al., 2016). Ne was loaded into the sample chamber as the pressure-transmitting medium using the COMPRES/GSECARS gas-loading system (Rivers et al., 2008). The uncertainties in pressures were propagated from the standard deviation of the unit-cell volumes of Au and Ne (if applicable). Angle-dispersive X-ray diffraction measurements were performed at beamline 13-BM-C of the APS, ANL. The incident X-ray beam had a monochromatic wavelength of 0.434 Å and was focused to ~15 × 15 μm^2. Two-dimensional X-ray diffraction images were recorded on a MAR165 CCD detector and the sample-to-detector distance and the tilt angle of the detector relative to the incident X-ray beam were calibrated using 1-bar diffraction of the NIST 660a LaB_6 standard. X-ray diffraction images of ε-Fe_7N_3, γ'-Fe_4N, and Fe were exposed for 60 s. At each pressure, the XRD patterns were integrated using Dioptas software (Prescher & Prakapenka, 2015). For selected pressures (lowest, highest, and one intermediate pressure), crystal structures were confirmed from XRD data using the full spectrum Le Bail fitting technique (Le Bail, 2012) implemented in the EXPGUI/GSAS software package (Toby, 2001).

3 Results

3.1 No structural transition of Fe_7N_3 or Fe_4N

XRD patterns for both iron nitrides within the investigated pressure range at 300 K show sharp and intense peaks from the sample, Au, Ne, and Re, and no new diffraction lines nor splitting of lines were observed. The lattice parameters of ε-Fe_7N_3 were obtained by fitting diffraction lines (002), (111) and (112), and that of γ'-Fe_4N was fit from diffraction lines (111) and (200) using PDIndexer (Seto et al., 2010). The uncertainty in the lattice parameters corresponds to one standard deviation obtained in fit using multiple XRD peaks. The pressure at each step was calculated from the lattice parameters of Au by fitting the diffraction lines (111) and (200), and from Ne by fitting (111) and (200) peaks at ~19-60 GPa as well (Table S1-3). The uncertainties of pressures were propagated from uncertainties of unit cell volumes of Au and Ne, and uncertainties of their equation of state parameters (Fei et al., 2007).

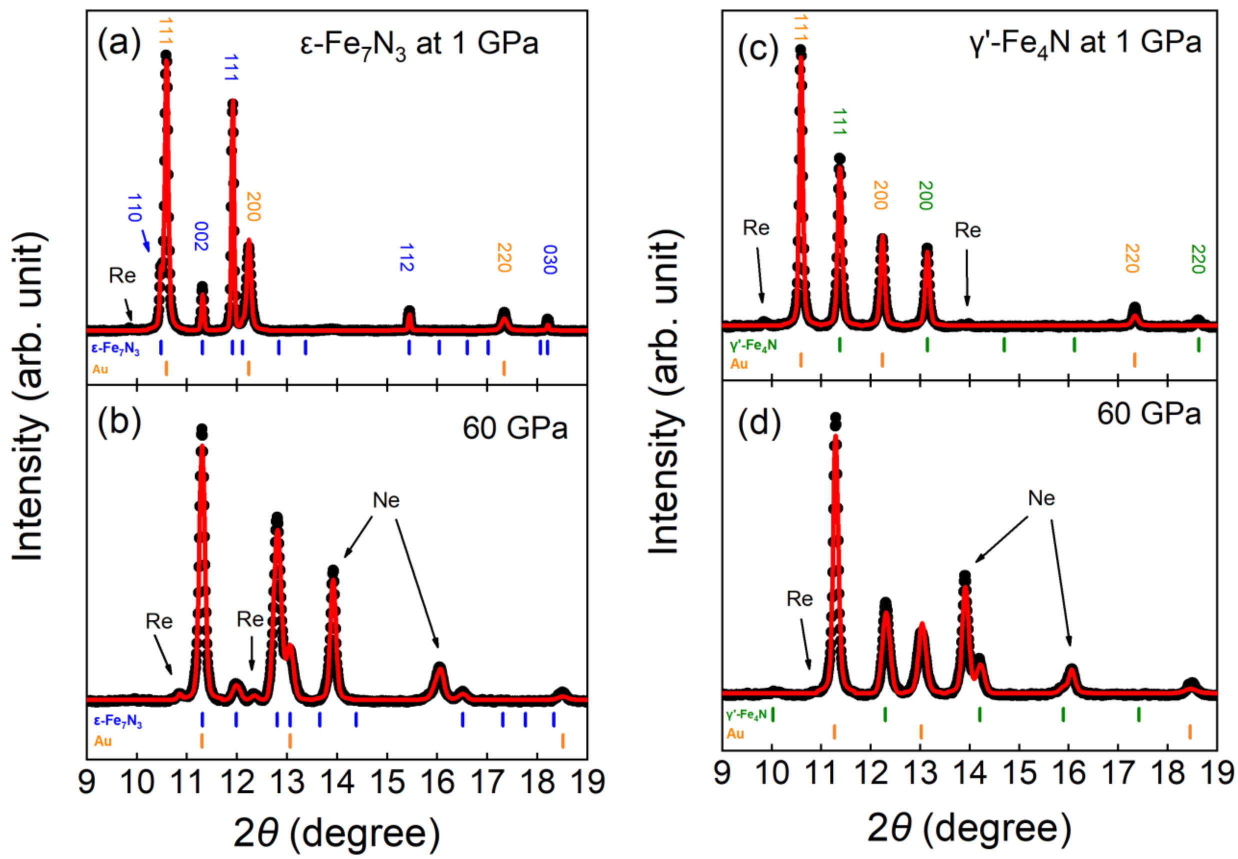

Figure 1. (a) and (b) are representative X-ray diffraction patterns of ε-Fe_7N_3 at 1 and 60 GPa at 300 K, respectively; (c) and (d) are representative X-ray diffraction patterns of γ'-Fe_4N at 1 and 60 GPa at 300 K, respectively. Le Bail refinements (red solid curves) of observed XRD data (black dots) were carried out after background subtraction, demonstrating all sample peaks match hexagonal ε-Fe_7N_3 and cubic γ'-Fe_4N, respectively, within the investigated pressure range. The vertical ticks are ε-Fe_7N_3 (blue), γ'-Fe_4N (dark green), and the pressure calibrant, Au (orange). The wavelength of the incident X-ray beam was 0.434 Å.

Diffraction data of ε-Fe_7N_3 were refined using a $P6_322$ space group (averaged wRp = 2.2 %, representatives shown in Figs. 1a and 1b) up to 60 GPa. Le Bail refinements of the structure of γ'-Fe_4N were performed with the $Pm\bar{3}m$ space group (averaged wRp = 1.8 %, representatives shown in Figs. 1c and 1d) up to 60 GPa. Note that previous work indicates that ε-Fe_7N_3 is metastable above ~40 GPa (Minobe et al., 2015), and γ'-Fe_4N is metastable above ~56 GPa (Breton et al., 2019). Both samples continue to adopt the initial structures without dissociation or phase transition up to 60 GPa at 300 K, but above 40 GPa we assume that ε-Fe_7N_3 is structurally metastable.

3.2 Spin states of ε-Fe_7N_3 and γ'-Fe_4N

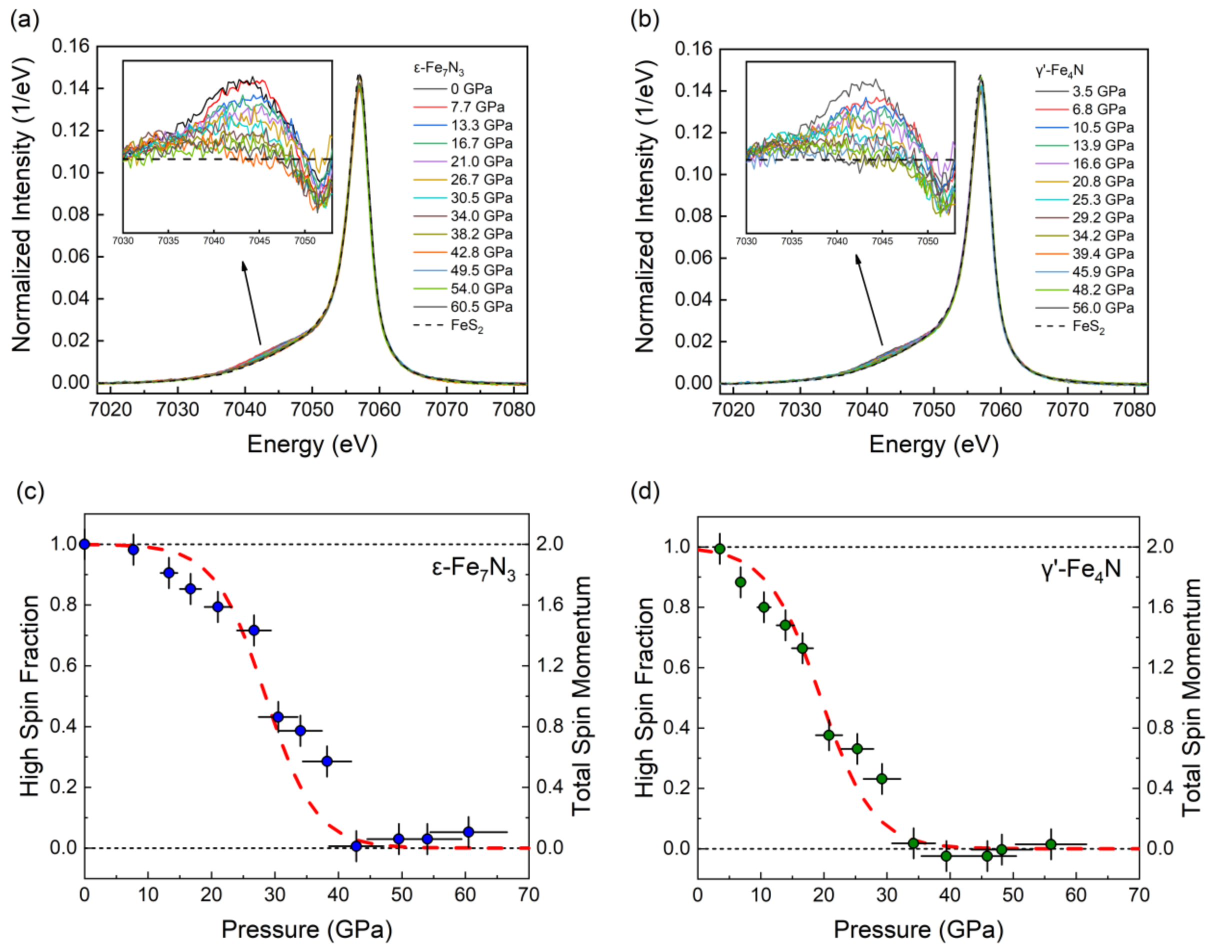

Figure 2. (a-b) Fe-K_β fluorescence spectra of ε-Fe_7N_3 and γ'-Fe_4N up to 60.5 GPa at 300 K. The XES spectra were normalized to unity in integrated intensity. The top-left inset shows intensity difference of observed satellite emission peak (K_β') between 7030 and 7053 eV relative to the low-spin reference FeS_2 at 0 GPa (black dashed line). (c-d) High-spin fraction of Fe in ε-Fe_7N_3 and γ'-Fe_4N as a function of pressure derived from the XES measurements following integrated relative difference method (Mao et al., 2014). Completion of the spin transition of ε-Fe_7N_3 is at ~40 GPa, and for γ'-Fe_4N at ~30 GPa. The dashed line is fitted by Boltzmann function, and error bars determined by comparing results using FeS_2 vs. sample at 60 GPa as low-spin references. Pressures were determined by ruby fluorescence (Mao et al., 1986) before and after each XES collection, which differed by up to 10% due to relaxation of the sample or cell assembly.

The net magnetic spin state of 3*d* electrons of Fe in ε-Fe_7N_3 and γ'-Fe_4N can be probed by XES spectra of the K_β fluorescence lines. At ambient conditions, the XES spectra for both iron nitrides are composed of a dominant $K_{\beta1,3}$ peak and a lower-energy satellite K_β' peak, as a result of the 3*p* core-hole-3*d* exchange interaction in the final state of the emission process, consistent with iron entirely in the high-spin state (Figs. 2a and 2b). The intensity of the satellite peak in the magnetic/high spin state is lower than that of iron oxides such as FeO and Fe_2O_3

(Badro et al., 2003; Badro et al., 2002), but similar to that of pure iron and iron alloys (such as Fe-C, Fe-P, Fe-S alloys). As pressure increases, the integrated K_β' peak intensity begins to decrease. The observed decrease demonstrates that the onsets of spin transitions in both compounds are nearly immediate upon compression and no higher than 10 GPa in ε-Fe_7N_3 and 5 GPa in γ'-Fe_4N. The integrated K_β' peak of ε-Fe_7N_3 and γ'-Fe_4N disappears at 43 and 34 GPa, respectively, with no further change up to 60 GPa (Figs. 2c and 2d). The decrease of total spin moment of Fe as a function of pressure illustrates both ε-Fe_7N_3 and γ'-Fe_4N undergo a gradual spin-pairing transition from high to low-spin state, with Fe in ε-Fe_7N_3 and γ'-Fe_4N fully in low-spin state at pressures higher than 43 and 34 GPa, respectively (Figs. 2c and 2d). Spin transition pressures are expected to be upper bounds due to possible effects of pressure hysteresis and non-hydrostatic stress on the spin crossover upon compression (Lin et al., 2013). Observed changes in XES spectra of ε-Fe_7N_3 and γ'-Fe_4N correspond to magnetic to nonmagnetic (high to low spin) transitions, but the ferromagnetic to paramagnetic transition, depending on the relative orientations of the individual spins, cannot be detected by XES. However, both ferromagnetic-paramagnetic and magnetic-nonmagnetic transitions may be detected via XRD if they take place and affect compressibility.

3.3 Compression behavior of ε-Fe_7N_3 and γ'-Fe_4N

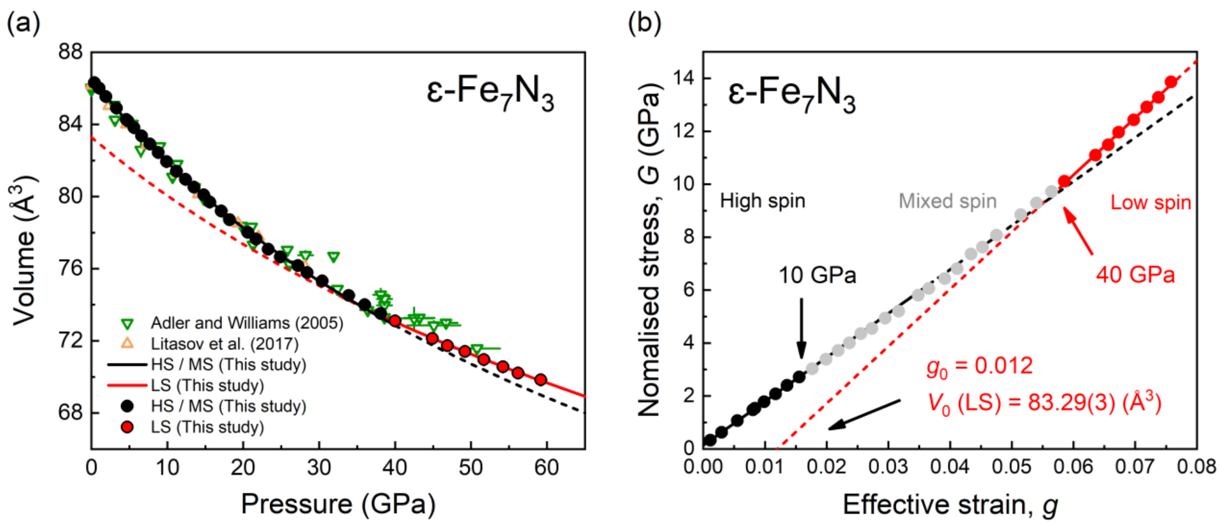

Figure 3. Compression behavior of ε-Fe_7N_3 at 300 K. (a) Unit-cell volume of ε-Fe_7N_3 up to 60 GPa at 300 K determined from X-ray diffraction measurements in this work (solid circles), together with previous experimental results. The black and red curves represent the 3rd-order Birch-Murnaghan equation of state (BM3-EoS) fits for the data for high spin (HS) and mixed spin (MS) / magnetic state (1 bar-40 GPa), low spin (LS) / nonmagnetic state (40-60 GPa), respectively. (b) Normalized stress G as a function of effective strain g. Solid black, gray, and red circles represent the results of high spin, mixed spin, and low spin state, respectively, as determined by XES. Black and red lines indicate fits of the high spin and low spin state $G(g)$ data, respectively. The V_0 for the nonmagnetic state is obtained by extrapolating g to g_0.

Pressure-volume (P-V) data obtained from XRD of ε-Fe_7N_3 and γ'-Fe_4N at 300 K demonstrate smooth compression without discontinuity in volume (Figs. 3a and 4a). Second-order and order-disorder transitions such as magnetic transitions may be continuous in volume but discontinuous in the higher-order derivatives of $P(V)$ (Vocadlo et al., 2002). Subtle effects on the unit cell volume with abrupt changes in incompressibility may be emphasized by the relationship between the Eulerian finite strain ($f_E = [(V_0/V)^{2/3}-1]/2$) versus the normalized stress ($F_E = P/[3f_E(1+2f_E)^{5/2}]$) (Angel, 2000) as in previous studies (Chen et al., 2012; Liu et al., 2016).

However, it is important to note that the calculation of both F_E and f_E requires priori knowledge of the 1-bar volume (V_0), and using an incorrect value of V_0 produces an anomalous curvature in the *f*-*F* plot (Angel, 2000). Thus, to avoid the bias caused by V_0 of the unquenchable nonmagnetic phase, we plot the effective strain ($g = [(V_0/V)^{2/3}-1]/2$), same as f_E, versus the normalized stress ($G = P/[3(1+2g)^{3/2}]$) following the formalism (Jeanloz, 1981) for ε-Fe_7N_3 and γ'-Fe_4N (Figs. 3b and 4b), respectively.

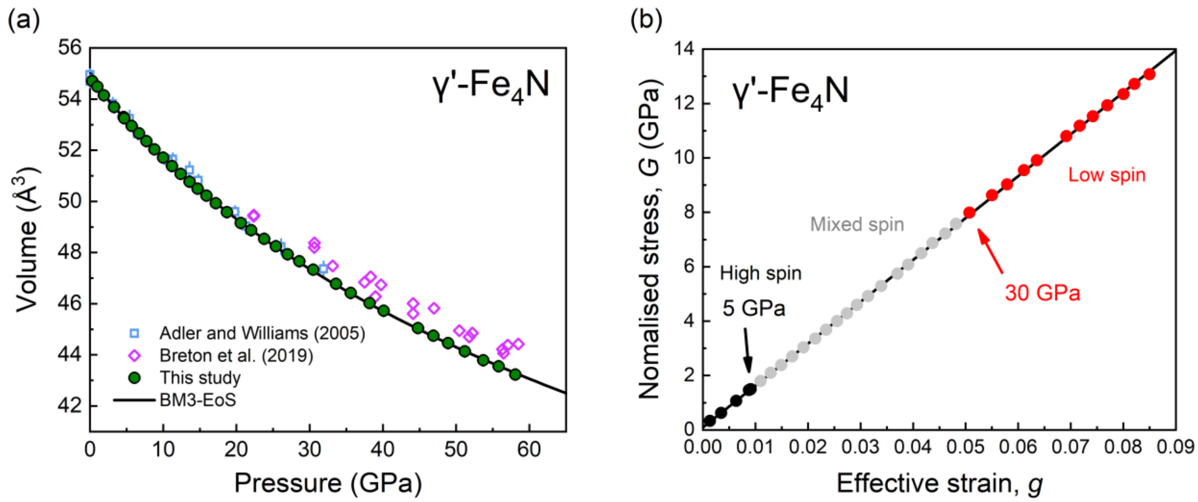

Figure 4. Compression behavior of γ'-Fe_4N at 300 K. (a) Unit-cell volume of γ'-Fe_4N up to 60 GPa at 300 K determined from X-ray diffraction measurements in this work (dark green circles), together with previous experimental results. The black curve represents the 3rd-order Birch-Murnaghan equation of state (BM-EoS) fit of all pressure-volume data from this study. (b) Normalized stress *G* as a function of effective strain *g*. Solid black, gray, and red circles represent the results of high spin, mixed spin, and low spin state, respectively, as determined by XES. The black solid line indicates a linear fit for all data. The pressure of onset and completion of spin transition is indicated by XES, but no change in compressibility can be observed in either plot.

As is shown in Fig. 3(b), the *g*-*G* plot of ε-Fe_7N_3 reveals that the pressure-dependent stress exhibits a linear response to applied strain up to 40 GPa within the established errors. Above 40 GPa, the slope of linearized *g*-*G* increases, implying a discontinuity of compression behavior and an increase in the incompressibility given that dG/dg is positively correlated with (K_0+P). This pressure is within the uncertainty of the completion of the magnetic to nonmagnetic transition (i.e., completion of spin transition) pressure of ~40 GPa determined independently by XES, indicating the elastic stiffening coincides with the magnetic collapse of Fe in ε-Fe_7N_3. In addition, this change of compressibility is similar to the pressure of ε- to β-Fe_7N_3 transition (Minobe et al., 2015) observed with laser-heating to promote equilibrium phase transitions. Due to the low pressure of the onset of the spin transition observed by XES, with upper bound ~10 GPa, and gradual, broad pressure range of the transition, it is difficult to resolve a transition from high to mixed spin state in the compression behavior. The compression behavior up to 40 GPa may thus represent the mixed-spin state. The crossing point of the *g* axis (i.e., $G = 0$) and the fitted curve constrain the zero-pressure volume of the nonmagnetic (or low spin state) phase to 83.29 ± 0.03 Å^3, with the error propagated from the error of linear fitting and volume at ambient conditions. No stiffening is observed at pressures lower than the spin transition pressure, so no clear evidence is available for any ferromagnetic-paramagnetic transition in ε-Fe_7N_3.

In contrast, the calculated *G* of γ'-Fe_4N can be linearized as a function of *g* within the investigated pressure range, and no discontinuity is observed (Fig. 4b). That is, both onset and completion of spin transition of Fe have little effect on the compression behavior γ'-Fe_4N, and no anomalous compressibility behavior needs to be explained by any other magnetic transition such as a ferromagnetic-paramagnetic transition.

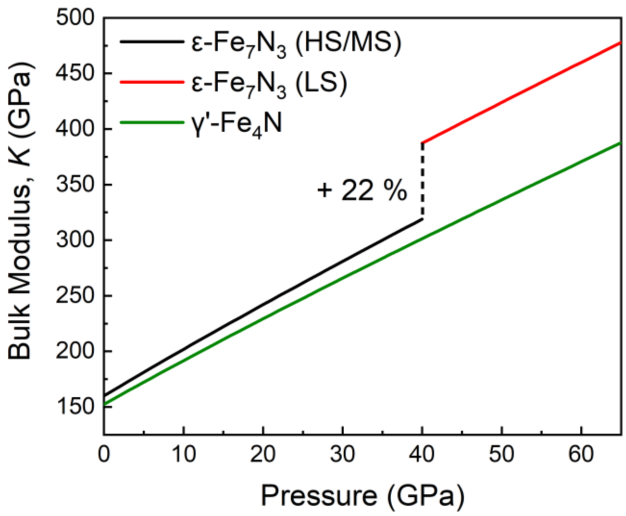

Figure 5. Isothermal bulk modulus (K) of high spin and mixed spin (magnetic) state ε-Fe_7N_3 (black curve), low spin (nonmagnetic) state ε-Fe_7N_3 (red curve), and γ'-Fe_4N (dark green curve) at 300 K as a function of pressure, calculated from the fitted BM-EOS parameters (Table 1). The magnetic to nonmagnetic transition of ε-Fe_7N_3 induces +22% increase in incompressibility at 40 GPa.

Discontinuities in higher derivatives of compression behavior can also be generated by nonhydrostatic stress in the sample chamber. To rule out this effect on iron nitrides, we consider the pressure gradient observed in Ne medium, microstrain in Au calibrant as determined by peak width, and the behavior of the Fe foil relative to previous measurements under quasi-hydrostatic conditions. The pressure difference determined from the Ne medium at positions of the two iron nitride samples is remains less than ~0.5 GPa up to the peak pressure of 60 GPa (Table S1-2), consistent with the low strength of Ne. Nonhydrostatic stress generally results in diffraction peak broadening due to microstrain (e.g., Takemura & Dewaele, 2008). We choose the Au (111) peak obtained at the γ'-Fe_4N sample position (Fig. 1c and d) to examine changes in diffraction peak width as a function of pressure. The normalized FWHM of the Au peak and its trend with pressure are comparable to previous measurements of Au foil and powder in He pressure medium (Takemura & Dewaele, 2008) (Fig. S2), indicating hydrostatic conditions up to 17 GPa and quasi-hydrostatic conditions at higher pressures, in agreement with previous characterization of the stress gradient sustained by the pressure medium Ne (Klotz et al., 2009). In addition, compression of both phases of pure Fe remains smooth over the entire pressure range and the condition of the phase transition and compressibility are in agreement with previous studies conducted under quasi-hydrostatic stress (e.g., Dewaele et al., 2006) (Fig. S1a). We investigated the P-V data and g-G plot of pure Fe loaded in the same sample chamber as a reference (Fig. S1). The discontinuities of both compression curve and g-G plot of Fe at ~15 GPa reflect a phase transition of α- to ε-Fe, which is in good agreement with previous studies (Dewaele et al., 2006). Therefore, the change in hydrostaticity of Ne at ~17 GPa (Fig. S2) was not manifested in the compression behavior of the samples, and the change in G-g at ~40 GPa of ε-Fe_7N_3 is not associated with nonhydrostaticity. Relative to previous studies (Adler & Williams, 2005; Litasov et al., 2017), the design of this study provides greater sensitivity to discontinuities in the compression behavior of ε-Fe_7N_3 due to denser data coverage with pressure intervals of ~1 GPa (Fig. 3a) and quasi-hydrostatic medium.

Given the compression and magnetic behaviors described above, we separately fit the *P*-*V* data of ε-Fe_7N_3 using third-order Birch-Murnaghan equation of state (BM3-EoS) over two distinct pressure ranges above and below 40 GPa, and that of γ'-Fe_4N with a single curve for the entire data range in order to better describe the compressibility. Below 40 GPa ε-Fe_7N_3 has a continuously-evolving, mixed-spin state, and the resulting EoS parameters are expected to be anomalously soft relative to the high-spin state. The parameters of the BM3-EoS, isothermal bulk modulus, K_0, its pressure derivative, K_0', and volume at 1 bar V_0, obtained in the present study and previous studies are summarized in Table 1.

The BM3-EoS parameters of magnetic, mixed spin ε-Fe_7N_3 obtained by fitting the *P*-*V* data from 1 bar and 40 GPa to BM3-EoS are compared with previous experimental constraints on the same stoichiometry (Adler & Williams, 2005; Litasov et al., 2017) (Table 1), showing consistency with the parameters obtained by (Litasov et al., 2017) within uncertainties, whereas 5% (or higher given the tradeoff between K_0 and K_0') elastic softer than that constrained by (Adler & Williams, 2005). Fig. 3a shows our measured *P*-*V* data are in good agreement with data obtained by (Litasov et al., 2017) from 1 bar to 31 GPa using a multi-anvil press, supporting a quasi-hydrostatic conditions in this study. However, the volume data reported by Adler and Williams (2005) deviate from our measurements at pressures higher than 30 GPa, likely due to the nonhydrostatic stress supported by methanol:ethanol:water pressure transmitting medium. Properties predicted for magnetic ε-$Fe_3N_{1.25}$ by density functional theory (Popov et al., 2015) are significantly offset, with V_0 lower by 6% and K_0 higher by 38% compared to experimental constraints. For nonmagnetic, low spin ε-Fe_7N_3, EoS fit for the data from 40 GPa to 60 GPa with a fixed V_0 [83.28(±2) Å^3] constrained by *g*-*G* plot (Fig. 3b) yields K_0 45% higher than that of magnetic phase (22% increase in bulk modulus at 40 GPa, Fig. 5), indicating a significant elastic stiffening associated with the magnetic collapse. Popov et al. (2015) predicted a magnetic-nonmagnetic transition of ε-Fe_7N_3 completed at 130 GPa, inducing a 35% difference in K_0, but both the transition pressure and bulk modulus are much higher than our constraints (Table 1). An increase in incompressibility induced by the collapse of magnetic momentum has been observed in other Fe-alloys such as Fe_3C (Prescher et al., 2012) and Fe_3P (Lai et al., 2020). These alloys are also not observed to soften during the spin transition, in contrast to pressure-induced Invar behavior of Fe alloys such as Fe-Ni (Dubrovinsky et al., 2001) and Fe_7C_3 (Chen et al., 2012) which undergo elastic softening during the transition followed by reaching a stiffer nonmagnetic state.

The EoS parameters of γ'-Fe_4N derived by fitting the measured *P*-*V* data up to 60 GPa to BM3-EoS agree with the parameters reported by Adler and Williams (2005) and (Guo et al., 2013) within uncertainties (Table 1). However, the K_0 reported by Breton et al. (2019), 169(±6) GPa, is 13% higher than our result, and the measured volumes deviate from our measurements as illustrated in Fig 4a. This discrepancy can be attributed to nonhydrostatic conditions in the sample chamber produced using KCl as the pressure transmitting medium, and lack of data at 0-20 GPa regime may cause a fitting bias when fixing the V_0 constrained by (Adler & Williams, 2005). K_0 computed by density functional theory with generalized gradient approximation studies (Niewa et al., 2009b; Popov et al., 2015) spans a range from 0 to 9% higher than that constrained by experiments, whereas the K_0 calculated from single-crystal elastic constants by first-principles total-energy method is 26% higher than that constrained by experiments.

Table 1. Equation of state parameters of ε-Fe_7N_3 and γ'-Fe_4N

Phase	Magnetism	*P* (GPa)	V_0 (Å^3)	K_0	K_0'	Method	Reference
ε-Fe_7N_3	Magnetic (mixed spin)	0-40	86.55(2)[a]	160(2)	4.3(2)	DAC[c]	This study
ε-Fe_7N_3	Nonmagnetic (low spin)	40-60	83.29(3)	232(9)	4.1(5)	DAC	This study
ε-Fe_7N_3	-	0-51	86.04(10)	168(10)	5.7(2)	DAC	Adler and Williams (2005)
ε-$Fe_3N_{1.26}$	-	0-31	86.18(3)	163(2)	5.3(2)	MA[d]	Litasov et al. (2017)
ε-$Fe_3N_{1.25}$	Magnetic (mixed spin)	0-100	81.35	224(1)	4.30(5)	DFT-GGA[e]	Popov et al. (2015)
ε-$Fe_3N_{1.25}$	Nonmagnetic	0-500	77.44	303(1)	4.38(1)	DFT-GGA	Popov et al. (2015)
γ'-Fe_4N	-	0-60	54.82(2)	152(2)	4.0(1)	DAC	This study
γ'-Fe_4N	-	0-31	54.95(22)	155(3)	4[b]	DAC	Adler and Williams (2005)
γ'-Fe_4N	-	0-33	54.81	154(3)	5.3(1)	DAC	Guo et al. (2013)
γ'-Fe_4N	-	22-60	54.95[b]	169(6)	4.1(4)	DAC	Breton et al. (2019)
γ'-Fe_4N	-	-	-	166(1)	4.2(1)	DFT-GGA	Niewa et al. (2009)
γ'-Fe_4N	Magnetic	-	54.64	192(1)	-	FP-TEC[f]	Gressmann et al. (2007)
γ'-Fe_4N	Magnetic (mixed spin)	0-200	54.10	152(4)	5.41(17)	DFT-GGA	Popov et al. (2015)
γ'-Fe_4N	Nonmagnetic	0-500	49.25	285(3)	4.38(1)	DFT-GGA	Popov et al. (2015)

[a] Numbers in parentheses are uncertainties on the last digits.
[b] Fixed value
[c] Diamond anvil cell
[d] Multi-anvil press
[e] Density functional theory -generalized gradient approximation
[f] First-principles total-energy calculations

Popov et al. (2015) predicted a magnetic-nonmagnetic transition of γ'-Fe_4N completed at 250 GPa, inducing an +87.5% jump of K_0, in contrast to our observation of this transition at much lower pressure with no significant effect on elasticity. γ'-Fe_4N is also less incompressible than both magnetic and nonmagnetic ε-Fe_7N_3, which leads to its destabilization at pressures above 60 GPa (Breton et al., 2019).

4 Discussion

4.1 Magnetic transitions of ε-Fe_7N_3 and γ'-Fe_4N

Both ε-Fe_7N_3 and γ'-Fe_4N adopt a ferromagnetic state at 1 bar with Curie temperatures of 400 K (Leineweber et al., 2001) and 750 K (Wriedt et al., 1987), respectively. Based on the XES observations described above, these compounds have fully reached a non-magnetic state by 43 and 34 GPa, respectively. Iron-light element compounds and alloys in Fe-P, Fe-C, Fe-S and other systems typically undergo a transition from ferromagnetic to paramagnetic state before the transition to a fully non-magnetic state (Chen et al., 2018; Chen et al., 2014; Gu et al., 2016; Lin et al., 2004a), so it can be inferred that an additional FM-PM transition may take place in Fe-N compounds below the completion of the spin transition. The only previous experimental investigation of pressure-induced magnetic transitions of iron nitrides was conducted by (Ishimatsu et al., 2003) on γ'-Fe_4N using XMCD, and showed the spin polarization was suppressed by pressure and finally vanished at 24 GPa. This loss of spin polarization was interpreted as a ferromagnetic to paramagnetic transition. This combined with our XES results indicates that paramagnetic γ'-Fe_4N has completely transitioned to the nonmagnetic state by 34 GPa. However, the pressure of any FM-PM transition in ε-Fe_7N_3 has not been directly observed by experiments, due to the lack of studies using Mössbauer spectroscopy or XMCD.

Indirect measurement of a FM-PM transition in Fe-N compounds through compression behavior has been inconclusive, and in iron-light element compounds more broadly, effects of FM-PM transitions on compressibility are either not observed or controversial. For example, the pressure of the FM-PM transition in Fe_3C was determined at ~8-10 GPa using Mössbauer spectroscopy, and no effect on the compression behavior was observed (Prescher et al., 2012); whereas Litasov et al. (2013) observed this transition at ~7-9 GPa by based on anomalous compression behavior of the *a*-axis, and proposed an elastic stiffening. Conditions of FM-PM transitions identified in previous work on ε-Fe_7N_3 and γ'-Fe_4N do not correspond to any significant changes in incompressibility.

In contrast, most Fe-light element compounds and alloys do exhibit stiffening after completing the transition to nonmagnetic state. Comparison between compression behavior and spin transition of ε-Fe_7N_3 reveals elastic stiffening associated with magnetic-nonmagnetic (i.e., high to low spin) transition at ~40 GPa. Similar behaviors have been observed and predicted in iron alloys, such as Fe-C, Fe-P, Fe-S systems (see section 4.2 for more discussion), which consistently show that the PM-NM transition induces elastic stiffening, whereas elastic softening of Fe_7C_3 is due to Invar behavior (Chen et al., 2012; Chen et al., 2014; Mookherjee et al., 2011). γ'-Fe_4N is unique among the Fe-light element compounds and alloys discussed here: while the pressure of the PM-NM transition is constrained through complementary spectroscopic methods, it has no significant effect on compression behavior.

Ab initio calculations of magnetic states of Fe-N compounds have predicted magnetic transition pressures much higher than those observed in experiments. The transitions from magnetic to non-magnetic states of ε-$Fe_3N_{1.25}$ and γ'-Fe_4N at 0 K were predicted to complete at 130 GPa and 250 GPa, respectively (Popov et al., 2015). Popov et al. (2015) also predicted significant volume collapse of iron nitrides due to the changes in the magnetic moment, which is in contrast to experimental observations, and not reported in previous *ab initio* calculations on iron carbides (Mookherjee et al., 2011; Vocadlo et al., 2002) although both studies used the generalized gradient approximation (GGA).

The difference in magneto-elastic coupling behavior between ε-Fe_7N_3 and γ'-Fe_4N may be attributed to the difference in strengths of Fe-N bonds associated with the crystal structures. In the idealized model of the crystal structure of ε-Fe_3N, the iron atoms are distributed according to hexagonal close packing (ε-Fe) and nitrogen atoms occupy one-third of octahedral voids between the iron layers in an ordered manner (Fig. S3). However, nonstoichiometric ε-Fe_3N_x ($0.75 < x < 1.4$) exhibits a broad homogeneity range together with some entropy-driven transfer of nitrogen to further octahedral voids (Niewa et al., 2009a). Iron atoms in γ'-Fe_4N are distributed according to the cubic close packing (γ-Fe) and nitrogen atoms occupy one-fourth of octahedral voids (Fig. S3). The resulting different 3*d* band structure affected by stronger 3*p*-3*d* hybridization of Fe and N in ε-Fe_7N_3 leads to a magnetic to nonmagnetic transition pressure of ε-Fe_7N_3 ~10 GPa higher than that observed in γ'-Fe_4N (Fig. 2). The difference in transition pressures may also be due to the relationship between anisotropic compressibility and the orientation of the magnetic moment relative to the crystal structure. For ε-Fe_7N_3, a collinear ferromagnetic arrangement of moments was determined to be parallel to the *c*-axis by neutron diffraction measurements (Robbins & White, 1964), and *c*-axis is more incompressible than *a*-axis (Shi et al., 2013) (*c*/*a* ratio increases with pressure, Fig. S4); while for γ'-Fe_4N, magnetic arrangement of moments was proposed to be parallel to the *a*-axis (Costa-Krämer et al., 2004), which is the stiffest direction (Gressmann et al., 2007). To better understand the effect of spin transition on elastic anisotropy of both iron nitrides, further measurements on elastic constants up to spin transition pressures are necessary.

4.2. Magneto-elastic coupling in Fe-light element alloys/compounds

Previous studies have identified multiple candidate Fe alloys and light element compounds that can match the observed density and elastic properties of Earth's core (reviewed by Hirose et al., 2013; Li & Fei, 2014), and many of them undergo pressure-induced magnetic transitions with effects on elasticity (reviewed by Caracas, 2016). As a result, the extrapolation of density and velocity of ambient or low-pressure data to Earth's core conditions may be misleading, and experiments at higher pressures and temperatures are critical. However, the pressure of magnetic collapse and its coupling with elastic properties were inconsistent in previous results: for example, the pressure of PM to NM transition for Fe_3C from different studies spans a large range of 22 to 68 GPa (reviewed by Chen & Li, 2016). This inconsistency is partially caused by different criteria for magnetic transitions constrained using different methods.

The spin transition (or PM - NM transition) of ionic or covalent materials is usually accompanied by a change in interatomic distance due to a decrease in the size of the Fe atom, which results in a volume collapse (Lin et al., 2013). In Fe alloys, the effect of the spin transition on structure and volume is subtle, leading to difficulties in detection. For direct comparison to this work on ε-Fe_7N_3 and γ'-Fe_4N, in which complementary methods determine the collapse of magnetic momentum and changes in compression behavior, we re-examine evidence for magnetic collapse and its effect on the compression behavior of other Fe-light element compounds Fe_3S, Fe_3P, Fe_7C_3, and Fe_3C, for which previous authors have obtained both XES measurements and dense *P-V* data coverage up to ~150 GPa.

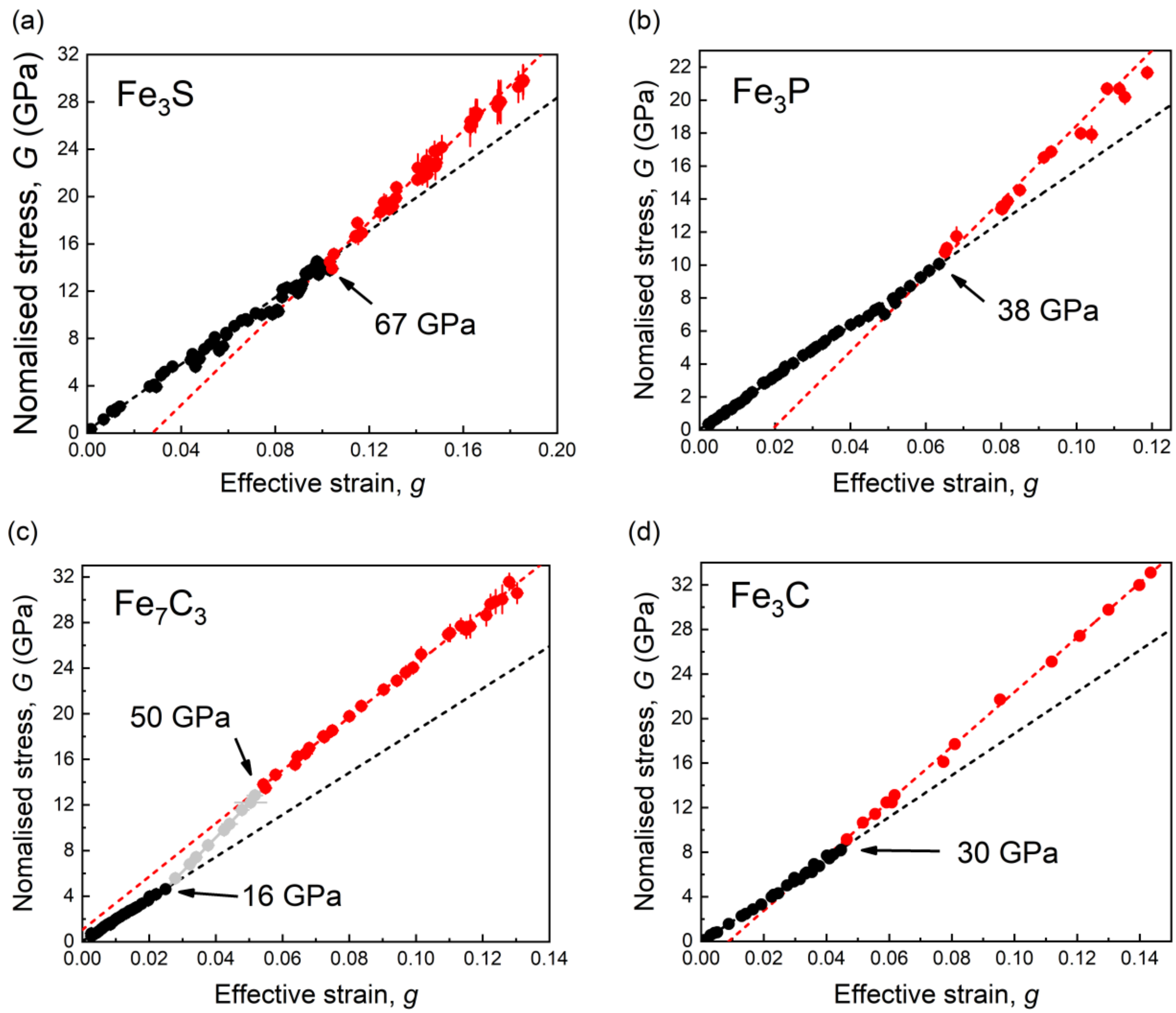

Figure 6. Normalized stress *G* as a function of effective strain *g* for (a) Fe_3S (Chen et al., 2007; Kamada et al., 2014; Seagle et al., 2006), (b) Fe_3P (Lai et al., 2020), (c) Fe_7C_3 (Chen et al., 2012; Liu et al., 2016), and (d) Fe_3C (Li et al., 2002; Litasov et al., 2013; Ono & Mibe, 2010; Sata et al., 2010). Dashed lines are linear fits to *g*-*G*, and the discontinuity in compression behavior corresponds to the change of slope of the linearized *g*-*G* plot.

Fe_3S remains in the tetragonal structure up to at least 200 GPa, with the completion of magnetic-nonmagnetic transition determined to occur at ~25 GPa by XES (Shen et al., 2003). A previous study argued that the magnetic transition did not affect the structure or compression behavior of Fe_3S (Kamada et al., 2014). However, a *g*-*G* plot (Fig. 6a) of the compression measurements from (Chen et al., 2007; Kamada et al., 2014; Seagle et al., 2006) illustrates a discontinuity in compression behavior at ~67 GPa, which could have been induced by a magnetic collapse. The spin transition pressure may be underestimated by XES (Shen et al., 2003), due to the limitations of the spectral analysis method (no low spin reference applied) and the limited pressure range (up to 30 GPa) of the study.

Fe_3P is isostructural with the Fe_3S tetragonal phase at ambient conditions, and in-situ XRD patterns suggest no structural phase transition up to 111 GPa (Lai et al., 2020), although the structural evolution of Fe_3P upon compression remains controversial (Gu et al., 2014;

Sagatov et al., 2020; Scott et al., 2007). The *g*-*G* plot based on the *P*-*V* measurements by (Lai et al., 2020) shows an increase in incompressibility at ~38 GPa (Fig. 6b), which coincides with the pressure of magnetic spin momentum collapse determined by XES (Gu et al., 2016). Lai et al. (2020) propose the completion of magnetic-nonmagnetic transition occurred at 21 GPa based on the disappearance of fast oscillation in Mössbauer spectra, which can be attributed to a ferromagnetic to paramagnetic transition.

Fe_7C_3 adopts a hexagonal structure from ~7-8 GPa to 167 GPa (Chen et al., 2012; Lord et al., 2009), and its magneto-elastic coupling effects have been thoroughly studied. By plotting the measurements from (Chen et al., 2012; Liu et al., 2016) as a *g*-*G* relation, an elastic stiffening occurs at 16 GPa and a softening occurs at 50 GPa (Fig. 6c). These discontinuities in the compression behavior can be explained by a noncollinear to paramagnetic transition proposed by (Liu et al., 2016) and a magnetic collapse determined by XES (Chen et al., 2014), respectively.

Fe_3C, known as the mineral cohenite, has an orthorhombic structure with *Pnma* space group, and no structural change in Fe_3C was observed up to 187 GPa (Sata et al., 2010). The pressure of PM-NM (or high- to low-spin) transition in Fe_3C determined by XES has ranged widely from ~25 GPa by (Lin et al., 2004b) to ~50 GPa by (Chen et al., 2018). The *g*-*G* plot of *P*-*V* measurements combined from (Li et al., 2002; Litasov et al., 2013; Ono & Mibe, 2010; Sata et al., 2010) indicates an elastic stiffening occurring at ~30 GPa (Fig. 6d), which is consistent with the decreasing of the emission satellite peak intensity until 30 GPa observed by (Lin et al., 2004b). We thus interpret the discontinuity in compression behavior of Fe_3C at ~30 GPa is induced by the completion of the spin transition.

In summary, XES and *g*-*G* plots generally reveal the collapse of magnetic moment and effects on the compression behavior of Fe-light element alloys and compounds, which are candidate constituents of the Earth' core. A change in incompressibility induced by magnetic-nonmagnetic transitions may be common throughout Fe-light element compound systems, whereas the effects from FM-PM transition on compression are not significant for most compounds. To extrapolate physical properties to conditions of Earth's core, low spin/nonmagnetic thermodynamic parameters should be used, and the effects of temperature should be considered. It has been shown that the pressure range for mixed-spin ferropericlase [$(Mg_{0.75}Fe_{0.25})O$] is broadened by 30 GPa as the temperature increases from 300 to 2000 K (Mao et al., 2011). The thermal equations of state of Fe-light element alloys up to Earth's core conditions await further investigation.

4.3. Implications for iron alloys in Earth's and planetary cores

Our results suggest that although magnetic-to-nonmagnetic transitions do not produce sharp discontinuities in the compression behavior of Fe_7N_3, Fe_3S, Fe_3P, Fe_7C_3, and Fe_3C, their effect is non-negligible and additional tools, such as XES experiments and an analysis of *g*-*G* plots, are required to accurately determine the pressure range of the magnetic transitions. Consequently, the effect of magnetic transitions on the compression behavior of other light-element-bearing iron compounds may have been overlooked in previous experiments based only on an analysis of the pressure-volume data (e.g., Kamada et al., 2014). The effects of magnetic transitions should not be ignored when investigating the roles of iron alloys in Earth's and planetary cores under relevant conditions.

For example, distribution of iron isotopes in the Earth, which has been used to trace planetary differentiation processes, is dependent on isotope fractionation between various candidate host phases for iron in planetary cores and silicate melts under different pressure, temperature, composition, and oxygen fugacity conditions (Dauphas et al., 2017). Pressure effects on iron isotope fractionation determined by nuclear resonant inelastic X-ray scattering spectroscopy measurements have been different for different alloys, which is explained by differences in bond strength between combinations of iron with different alloying elements (Liu et al., 2017; Shahar et al., 2016). Considering the effects of magnetic transitions on bond lengths and strengths of iron alloys presented in this study, magnetic transitions of iron alloys may impact the pressure dependence of the $^{57/54}$Fe β factor (reduced partition function ratios) and thus the iron isotope fractionation over Earth's history.

The pressure conditions of the magnetic transitions in ε-Fe_7N_3, Fe_3S, Fe_3P, Fe_7C_3, and Fe_3C revealed by this study overlap with the moderate *P-T* range of the cores of relatively small planets, such as Mercury (~8 to 40 GPa, ~1700 to 2200 K) (Chen et al., 2008) and Mars (~24 to 42 GPa, ~2000 to 2600 K) (Fei & Bertka, 2005). Whether Mercury and Mars have fully molten cores (Margot et al., 2007; Yoder et al., 2003) or include solid inner cores (Genova et al., 2019; Stevenson, 2001) is under debate. In either case, planetary cooling may entail a present and/or past "snowing-core" scenario where iron-rich solids nucleate at the liquidus and sink or rise based on buoyancy. Minor solid iron alloys may thus significantly affect planetary core dynamics through powering magnetic dynamos (Breuer et al., 2015 and references therein). The effects of magnetic transition on physical properties [such as incompressibility and density (Fig. S5)] of these candidate constituents of planetary cores may play an important role in deciphering the potential role of N, C, S, and P in these planetary cores.

5 Conclusions

In this work, we report spin/magnetic transitions and compressibility of ε-Fe_7N_3 and γ'-Fe_4N, the two stable iron nitrides at ambient conditions. Synchrotron XES and XRD measurements were carried out up to 60 GPa at 300 K using DAC. The completion of magnetic collapse in ε-Fe_7N_3 and γ'-Fe_4N is observed at 43 and 34 GPa, respectively, indicated by the completion of high- to low-spin state transition. Comparing spin transition and discontinuities in compression behavior monitored by *g-G* plot, the completion of spin transition induces elastic stiffening in ε-Fe_7N_3 by 22% at ~40 GPa, but has no resolvable effect on the compression behavior of γ'-Fe_4N. Accordingly, fitting *P-V* data to BM3-EoS yields: V_0 = 86.55±0.02 (Å^3), K_0 = 160 ± 2 GPa, and K_0' = 4.3 ± 0.2 for magnetic, mixed spin ε-Fe_7N_3; V_0 = 83.29 ± 0.03 (Å^3), K_0 = 232 ± 9 GPa, and K_0' = 4.1 ± 0.5 for nonmagnetic, low spin ε-Fe_7N_3; V_0 = 54.82 ± 0.02 (Å^3), K_0 = 152 ± 2 GPa, and K_0' = 4.0 ± 0.1 for γ'-Fe_4N within the investigated pressure range.

Using the same protocol, we re-examine evidence for magnetic collapse and its effect on the compression behavior of other Fe-light element compounds as candidate components of terrestrial planet's core, Fe_3S, Fe_3P, Fe_7C_3, and Fe_3C. We summarize previous reported dense *P-V* data up to ~150 GPa and comparing with XES measurements, which indicate the completion of the magnetic transition in Fe_3S, Fe_3P, and Fe_7C_3 is at about 67, 38, 50, and 30 GPa, respectively. The completion of the magnetic transition of Fe_3S and Fe_3P induces elastic stiffening, whereas that of Fe_7C_3 induces elastic softening. The changes of incompressibility induced by magnetic-nonmagnetic transition may have potential implications in deciphering the role of iron-light element alloys in Earth's and planetary cores.

Acknowledgments

We thank two anonymous reviewers for constructive comments and suggestions that improved the manuscript, and Dr. Stephen Parman for editorial handing and comments. S. M. Dorfman acknowledges support for this work from NSF EAR-1751664. J. Li acknowledges support from NSF EAR-1763189 and AST-1344133. Beamtime for XES was provided through the Capital-DOE Alliance Center. XES measurements were performed at HPCAT (Sector 16), Advanced Photon Source (APS), Argonne National Laboratory. HPCAT operations are supported by DOE-NNSA's Office of Experimental Sciences. XRD measurements performed at GeoSoilEnviroCARS (The University of Chicago, Sector 13), Advanced Photon Source (APS), Argonne National Laboratory. GeoSoilEnviroCARS is supported by the National Science Foundation-Earth Sciences (EAR-1634415) and Department of Energy-GeoSciences (DE-FG02-94ER14466). Use of the COMPRES-GSECARS gas loading system and the PX2 program was supported by COMPRES under NSF Cooperative Agreement EAR -1606856 and by GSECARS through NSF grant EAR-1634415 and DOE grant DE-FG02-94ER14466. This research used resources of the Advanced Photon Source, a U.S. Department of Energy (DOE) Office of Science User Facility operated for the DOE Office of Science by Argonne National Laboratory under Contract No. DE-AC02-06CH11357. All the data to produce the results are available on Zenodo (https://doi.org/10.5281/zenodo.3959348).

References

Adler, J. F., & Williams, Q. (2005). A high-pressure X-ray diffraction study of iron nitrides: Implications for Earth's core. *Journal of Geophysical Research-Solid Earth, 110*(B1). http://10.1029/2004jb003103

Angel, R. J. (2000). Equations of state. *High-Temperature and High-Pressure Crystal Chemistry, 41*(1), 35-59. http://10.2138/rmg.2000.41.2

Badro, J., Fiquet, G., Guyot, F., Rueff, J. P., Struzhkin, V. V., Vanko, G., & Monaco, G. (2003). Iron partitioning in Earth's mantle: toward a deep lower mantle discontinuity. *Science, 300*(5620), 789-791. http://10.1126/science.1081311

Badro, J., Fiquet, G., Struzhkin, V. V., Somayazulu, M., Mao, H. K., Shen, G., & Le Bihan, T. (2002). Nature of the high-pressure transition in Fe_2O_3 hematite. *Physical Review Letters, 89*(20), 205504. http://10.1103/PhysRevLett.89.205504

Badro, J., Rueff, J. P., Vanko, G., Monaco, G., Fiquet, G., & Guyot, F. (2004). Electronic transitions in perovskite: possible nonconvecting layers in the lower mantle. *Science, 305*(5682), 383-386. http://10.1126/science.1098840

Birch, F. (1952). Elasticity and constitution of the Earth's interior. *Journal of Geophysical Research, 57*(2), 227-286. http://10.1029/JZ057i002p00227

Breton, H., Komabayashi, T., Thompson, S., Potts, N., McGuire, C., Suehiro, S., et al. (2019). Static compression of Fe_4N to 77 GPa and its implications for nitrogen storage in the deep Earth. *American Mineralogist, 104*(12), 1781-1787. http://10.2138/am-2019-7065

Breuer, D., Rueckriemen, T., & Spohn, T. (2015). Iron snow, crystal floats, and inner-core growth: modes of core solidification and implications for dynamos in terrestrial planets and moons. *Progress in Earth and Planetary Science, 2*(1). http://10.1186/s40645-015-0069-y

Caracas, R. (2016). Crystal structures of Core materials. *Deep Earth: Physics and Chemistry of the Lower Mantle and Core, 217*, 57-68.

Chen, B., Gao, L., Funakoshi, K., & Li, J. (2007). Thermal expansion of iron-rich alloys and implications for the Earth's core. *Proceedings of the National Academy of Sciences, 104*(22), 9162-9167. http://10.1073/pnas.0610474104

Chen, B., Gao, L. L., Lavina, B., Dera, P., Alp, E. E., Zhao, J. Y., & Li, J. (2012). Magneto-elastic coupling in compressed Fe_7C_3 supports carbon in Earth's inner core. *Geophysical Research Letters, 39*(18). http://10.1029/2012gl052875

Chen, B., Lai, X. J., Li, J., Liu, J. C., Zhao, J. Y., Bi, W. L., et al. (2018). Experimental constraints on the sound velocities of cementite Fe_3C to core pressures. *Earth and Planetary Science Letters, 494*, 164-171. http://10.1016/j.epsl.2018.05.002

Chen, B., & Li, J. (2016). Carbon in the core. *Deep Earth: Physics and Chemistry of the Lower Mantle and Core*, 277-288.

Chen, B., Li, J., & Hauck, S. A. (2008). Non-ideal liquidus curve in the Fe-S system and Mercury's snowing core. *Geophysical Research Letters, 35*(7). http://10.1029/2008gl033311

Chen, B., Li, Z., Zhang, D., Liu, J., Hu, M. Y., Zhao, J., et al. (2014). Hidden carbon in Earth's inner core revealed by shear softening in dense Fe_7C_3. *Proceedings of the National Academy of Sciences, 111*(50), 17755-17758. http://10.1073/pnas.1411154111

Costa-Krämer, J. L., Borsa, D. M., García-Martín, J. M., Martín-González, M. S., Boerma, D. O., & Briones, F. (2004). Structure and magnetism of single-phase epitaxialγ′−Fe4N. *Physical Review B, 69*(14). http://10.1103/PhysRevB.69.144402

Dauphas, N., John, S. G., & Rouxel, O. (2017). Iron isotope systematics. *Reviews in Mineralogy and Geochemistry, 82*(1), 415-510.

De Waele, S., Lejaeghere, K., Leunis, E., Duprez, L., & Cottenier, S. (2019). A first-principles reassessment of the Fe-N phase diagram in the low-nitrogen limit. *Journal of Alloys and Compounds, 775*, 758-768. http://10.1016/j.jallcom.2018.09.356

Dewaele, A., Loubeyre, P., Occelli, F., Mezouar, M., Dorogokupets, P. I., & Torrent, M. (2006). Quasihydrostatic equation of state of iron above 2 Mbar. *Physical Review Letters, 97*(21), 215504. http://10.1103/PhysRevLett.97.215504

Dirba, I., Yazdi, M. B., Radetinac, A., Komissinskiy, P., Flege, S., Gutfleisch, O., & Alff, L. (2015). Growth, structure, and magnetic properties of γ'-FeN_4 thin films. *Journal of Magnetism and Magnetic Materials, 379*, 151-155. http://10.1016/j.jmmm.2014.12.033

dos Santos, A. V., & Samudio Pérez, C. A. (2016). Ab initio investigation of the substitution effects of 2*p* elements on the electronic structure of γ-Fe_4X (X = B, C, N, and O) in the ground state. *Journal of Materials Research, 31*(2), 202-212. http://10.1557/jmr.2015.394

Dubrovinsky, L., Dubrovinskaia, N., Abrikosov, I. A., Vennstrom, M., Westman, F., Carlson, S., et al. (2001). Pressure-induced Invar effect in Fe-Ni alloys. *Physical Review Letters, 86*(21), 4851-4854. http://10.1103/PhysRevLett.86.4851

Dziewonski, A. M., & Anderson, D. L. (1981). Preliminary Reference Earth Model. *Physics of the Earth and Planetary Interiors, 25*(4), 297-356. http://10.1016/0031-9201(81)90046-7

Fei, Y., & Bertka, C. (2005). Planetary science. The interior of Mars. *Science, 308*(5725), 1120-1121. http://10.1126/science.1110531

Fei, Y., Ricolleau, A., Frank, M., Mibe, K., Shen, G., & Prakapenka, V. (2007). Toward an internally consistent pressure scale. *Proceedings of the National Academy of Sciences, 104*(22), 9182-9186. http://10.1073/pnas.0609013104

Genova, A., Goossens, S., Mazarico, E., Lemoine, F. G., Neumann, G. A., Kuang, W., et al. (2019). Geodetic Evidence That Mercury Has A Solid Inner Core. *Geophysical Research Letters, 46*(7), 3625-3633. http://10.1029/2018gl081135

Gressmann, T., Wohlschlögel, M., Shang, S., Welzel, U., Leineweber, A., Mittemeijer, E. J., & Liu, Z. K. (2007). Elastic anisotropy of γ'-Fe_4N and elastic grain interaction in γ'-Fe_4N_{1-y} layers on α-Fe: First-principles calculations and diffraction stress measurements. *Acta Materialia, 55*(17), 5833-5843. http://10.1016/j.actamat.2007.07.001

Gu, T., Fei, Y., Wu, X., & Qin, S. (2014). High-pressure behavior of Fe_3P and the role of phosphorus in planetary cores. *Earth and Planetary Science Letters, 390*, 296-303. http://10.1016/j.epsl.2014.01.019

Gu, T., Fei, Y., Wu, X., & Qin, S. (2016). Phase stabilities and spin transitions of $Fe_3(S_{1-x}P_x)$ at high pressure and its implications in meteorites. *American Mineralogist, 101*(1), 205-210. http://10.2138/am-2016-5466

Guo, K., Rau, D., von Appen, J., Prots, Y., Schnelle, W., Dronskowski, R., et al. (2013). High pressure high-temperature behavior and magnetic properties of Fe_4N: experiment and theory. *High Pressure Research, 33*(3), 684-696. http://10.1080/08957959.2013.809715

Hirose, K., Labrosse, S., & Hernlund, J. (2013). Composition and State of the Core. In R. Jeanloz (Ed.), *Annual Review of Earth and Planetary Sciences, Vol 41* (Vol. 41, pp. 657-691). Palo Alto: Annual Reviews.

Hrubiak, R., Sinogeikin, S., Rod, E., & Shen, G. (2015). The laser micro-machining system for diamond anvil cell experiments and general precision machining applications at the High Pressure Collaborative Access Team. *Review of Scientific Instruments, 86*(7), 072202. Article. http://10.1063/1.4926889

Ishimatsu, N., Maruyama, H., Kawamura, N., Suzuki, M., Ohishi, Y., Ito, M., et al. (2003). Pressure-induced magnetic transition in Fe_4N probed by Fe *K*-edge XMCD measurement. *Journal of the Physical Society of Japan, 72*(9), 2372-2376. http://10.1143/JPSJ.72.2372

Jeanloz, R. (1981). Finite-Strain Equation of State for High-Pressure Phases. *Geophysical Research Letters, 8*(12), 1219-1222. http://10.1029/GL008i012p01219

Kamada, S., Ohtani, E., Terasaki, H., Sakai, T., Takahashi, S., Hirao, N., & Ohishi, Y. (2014). Equation of state of Fe_3S at room temperature up to 2 megabars. *Physics of the Earth and Planetary Interiors, 228*, 106-113. http://10.1016/j.pepi.2013.11.001

Kaminsky, F., & Wirth, R. (2017). Nitrides and carbonitrides from the lowermost mantle and their importance in the search for Earth's "lost" nitrogen. *American Mineralogist, 102*(8), 1667-1676. http://10.2138/am-2017-6101

Klotz, S., Chervin, J. C., Munsch, P., & Le Marchand, G. (2009). Hydrostatic limits of 11 pressure transmitting media. *Journal of Physics D-Applied Physics, 42*(7), 075413. http://10.1088/0022-3727/42/7/075413

Kusakabe, M., Hirose, K., Sinmyo, R., Kuwayama, Y., Ohishi, Y., & Helffrich, G. (2019). Melting Curve and Equation of State of β-Fe_7N_3: Nitrogen in the Core? *Journal of Geophysical Research: Solid Earth*. http://10.1029/2018jb015823

Lai, X., Zhu, F., Liu, Y., Bi, W., Zhao, J., Alp, E. E., et al. (2020). Elastic and magnetic properties of Fe_3P up to core pressures: Phosphorus in the Earth's core. *Earth and Planetary Science Letters, 531*, 115974. http://10.1016/j.epsl.2019.115974

Le Bail, A. (2012). Whole powder pattern decomposition methods and applications: A retrospection. *Powder Diffraction, 20*(4), 316-326. http://10.1154/1.2135315

Leineweber, A., Jacobs, H., Hüning, F., Lueken, H., & Kockelmann, W. (2001). Nitrogen ordering and ferromagnetic properties of ϵ-Fe_3N_{1+x} ($0.10\leq x\leq 0.39$) and ϵ-$Fe_3(N_{0.80}C_{0.20})_{1.38}$. *Journal of Alloys and Compounds, 316*(1-2), 21-38. http://10.1016/S0925-8388(00)01435-3

Li, J., & Fei, Y. (2014). Experimental Constraints on Core Composition. In H. D. Holland & K. K. Turekian (Eds.), *Treatise on Geochemistry* (pp. 527-557). Oxford: Elsevier.

Li, J., Mao, H. K., Fei, Y., Gregoryanz, E., Eremets, M., & Zha, C. S. (2002). Compression of Fe_3C to 30 GPa at room temperature. *Physics and Chemistry of Minerals, 29*(3), 166-169. http://10.1007/s00269-001-0224-4

Lin, J.-F., Fei, Y., Sturhahn, W., Zhao, J., Mao, H.-k., & Hemley, R. J. (2004a). Magnetic transition and sound velocities of Fe_3S at high pressure: implications for Earth and planetary cores. *Earth and Planetary Science Letters, 226*(1-2), 33-40. http://10.1016/j.epsl.2004.07.018

Lin, J. F., Speziale, S., Mao, Z., & Marquardt, H. (2013). Effects of the Electronic Spin Transitions of Iron in Lower Mantle Minerals: Implications for Deep Mantle Geophysics and Geochemistry. *Reviews of Geophysics, 51*(2), 244-275. http://10.1002/rog.20010

Lin, J. F., Struzhkin, V. V., Mao, H. K., Hemley, R. J., Chow, P., Hu, M. Y., & Li, J. (2004b). Magnetic transition in compressed Fe_3C from x-ray emission spectroscopy. *Physical Review B, 70*(21). http://10.1103/PhysRevB.70.212405

Litasov, K. D., Sharygin, I. S., Dorogokupets, P. I., Shatskiy, A., Gavryushkin, P. N., Sokolova, T. S., et al. (2013). Thermal equation of state and thermodynamic properties of iron carbide Fe_3C to 31 GPa and 1473 K. *Journal of Geophysical Research-Solid Earth, 118*(10), 5274-5284. http://10.1002/2013jb010270

Litasov, K. D., Shatskiy, A., Ponomarev, D. S., & Gavryushkin, P. N. (2017). Equations of state of iron nitrides ε-Fe_3N_x and γ-Fe_4N_y to 30 GPa and 1200 K and implication for nitrogen in the Earth's core. *Journal of Geophysical Research: Solid Earth*. http://10.1002/2017JB014059

Liu, J., Dauphas, N., Roskosz, M., Hu, M. Y., Yang, H., Bi, W., et al. (2017). Iron isotopic fractionation between silicate mantle and metallic core at high pressure. *Nature Communications, 8*, 14377. http://10.1038/ncomms14377

Liu, J., Dorfman, S. M., Lv, M., Li, J., Zhu, F., & Kono, Y. (2019). Loss of immiscible nitrogen from metallic melt explains Earth's missing nitrogen. *Geochemical Perspectives Letters*, 18-22. http://10.7185/geochemlet.1919

Liu, J. C., Li, J., & Ikuta, D. (2016). Elastic softening in Fe_7C_3 with implications for Earth's deep carbon reservoirs. *Journal of Geophysical Research-Solid Earth, 121*(3), 1514-1524. Article. http://10.1002/2015jb012701

Lord, O. T., Walter, M. J., Dasgupta, R., Walker, D., & Clark, S. M. (2009). Melting in the Fe–C system to 70 GPa. *Earth and Planetary Science Letters, 284*(1-2), 157-167. http://10.1016/j.epsl.2009.04.017

Mao, H. K., Xu, J., & Bell, P. M. (1986). Calibration of the ruby pressure gauge to 800 Kbar under quasi-hydrostatic conditions. *Journal of Geophysical Research-Solid Earth and Planets, 91*(B5), 4673-4676. http://10.1029/JB091iB05p04673

Mao, Z., Lin, J. F., Liu, J., & Prakapenka, V. B. (2011). Thermal equation of state of lower-mantle ferropericlase across the spin crossover. *Geophysical Research Letters, 38*(23). http://10.1029/2011gl049915

Mao, Z., Lin, J. F., Yang, J., Wu, J. J., Watson, H. C., Xiao, Y. M., et al. (2014). Spin and valence states of iron in Al-bearing silicate glass at high pressures studied by synchrotron Mossbauer and X-ray emission spectroscopy. *American Mineralogist, 99*(2-3), 415-423. http://10.2138/am.2014.4490

Margot, J. L., Peale, S. J., Jurgens, R. F., Slade, M. A., & Holin, I. V. (2007). Large longitude libration of Mercury reveals a molten core. *Science, 316*(5825), 710-714. http://10.1126/science.1140514

Mcdonough, W. F., & Sun, S. S. (1995). The Composition of the Earth. *Chemical Geology, 120*(3-4), 223-253. http://10.1016/0009-2541(94)00140-4

Minobe, S., Nakajima, Y., Hirose, K., & Ohishi, Y. (2015). Stability and compressibility of a new iron-nitride β-Fe_7N_3 to core pressures. *Geophysical Research Letters, 42*(13), 5206-5211. http://10.1002/2015gl064496

Mookherjee, M., Nakajima, Y., Steinle-Neumann, G., Glazyrin, K., Wu, X. A., Dubrovinsky, L., et al. (2011). High-pressure behavior of iron carbide (Fe_7C_3) at inner core conditions. *Journal of Geophysical Research-Solid Earth, 116*(B4). http://10.1029/2010jb007819

Nakajima, Y., Takahashi, E., Sata, N., Nishihara, Y., Hirose, K., Funakoshi, K., & Ohishi, Y. (2011). Thermoelastic property and high-pressure stability of Fe_7C_3: Implication for iron-carbide in the Earth's core. *American Mineralogist, 96*(7), 1158-1165. http://10.2138/am.2011.3703

Niewa, R., Rau, D., Wosylus, A., Meier, K., Hanfland, M., Wessel, M., et al. (2009a). High-pressure, high-temperature single-crystal growth, ab initio electronic structure calculations, and equation of state of ε-Fe_3N_{1+x}. *Chemistry of Materials, 21*(2), 392-398.

Niewa, R., Rau, D., Wosylus, A., Meier, K., Wessel, M., Hanfland, M., et al. (2009b). High-pressure high-temperature phase transition of γ′-Fe_4N. *Journal of Alloys and Compounds, 480*(1), 76-80. http://10.1016/j.jallcom.2008.09.178

Ono, S., & Mibe, K. (2010). Magnetic transition of iron carbide at high pressures. *Physics of the Earth and Planetary Interiors, 180*(1-2), 1-6. http://10.1016/j.pepi.2010.03.008

Poirier, J.-P. (1994). Light elements in the Earth's outer core: A critical review. *Physics of the Earth and Planetary Interiors, 85*(3-4), 319-337. http://10.1016/0031-9201(94)90120-1

Popov, Z. I., Litasov, K. D., Gavryushkin, P. N., Ovchinnikov, S. G., & Fedorov, A. S. (2015). Theoretical study of γ′-Fe_4N and ε-Fe_xN iron nitrides at pressures up to 500 GPa. *JETP Letters, 101*(6), 371-375. http://10.1134/s0021364015060090

Prescher, C., Dubrovinsky, L., McCammon, C., Glazyrin, K., Nakajima, Y., Kantor, A., et al. (2012). Structurally hidden magnetic transitions in Fe_3C at high pressures. *Physical Review B, 85*(14). http://10.1103/PhysRevB.85.140402

Prescher, C., & Prakapenka, V. B. (2015). DIOPTAS: a program for reduction of two-dimensional X-ray diffraction data and data exploration. *High Pressure Research, 35*(3), 223-230. http://10.1080/08957959.2015.1059835

Rivers, M., Prakapenka, V. B., Kubo, A., Pullins, C., Holl, C. M., & Jacobsen, S. D. (2008). The COMPRES/GSECARS gas-loading system for diamond anvil cells at the Advanced Photon Source. *High Pressure Research, 28*(3), 273-292. http://10.1080/08957950802333593

Robbins, M., & White, J. G. (1964). Magnetic Properties of Epsilon-Iron Nitride. *Journal of Physics and Chemistry of Solids, 25*(7), 717-&. http://Doi 10.1016/0022-3697(64)90182-9

Rubin, A. E., & Ma, C. (2017). Meteoritic minerals and their origins. *Geochemistry, 77*(3), 325-385. http://10.1016/j.chemer.2017.01.005

Sagatov, N., Gavryushkin, P. N., Inerbaev, T. M., & Litasov, K. D. (2019). New high-pressure phases of Fe_7N_3 and Fe_7C_3 stable at Earth's core conditions: evidences for carbon–nitrogen isomorphism in Fe-compounds. *RSC Advances, 9*(7), 3577-3581. http://10.1039/c8ra09942a

Sagatov, N. E., Gavryushkin, P. N., Banayev, M. V., Inerbaev, T. M., & Litasov, K. D. (2020). Phase relations in the Fe-P system at high pressures and temperatures from ab initio computations. *High Pressure Research, 40*(2), 235-244. http://10.1080/08957959.2020.1740699

Sakai, T., Takahashi, S., Nishitani, N., Mashino, I., Ohtani, E., & Hirao, N. (2014). Equation of state of pure iron and $Fe_{0.9}Ni_{0.1}$ alloy up to 3 Mbar. *Physics of the Earth and Planetary Interiors, 228*, 114-126. http://10.1016/j.pepi.2013.12.010

Sata, N., Hirose, K., Shen, G., Nakajima, Y., Ohishi, Y., & Hirao, N. (2010). Compression of FeSi, Fe_3C, $Fe_{0.95}O$, and FeS under the core pressures and implication for light element in the Earth's core. *Journal of Geophysical Research, 115*(B9). http://10.1029/2009jb006975

Scott, H. P., Huggins, S., Frank, M. R., Maglio, S. J., Martin, C. D., Meng, Y., et al. (2007). Equation of state and high-pressure stability of Fe_3P-schreibersite: Implications for phosphorus storage in planetary cores. *Geophysical Research Letters, 34*(6). http://10.1029/2006gl029160

Seagle, C. T., Campbell, A. J., Heinz, D. L., Shen, G., & Prakapenka, V. B. (2006). Thermal equation of state of Fe_3S and implications for sulfur in Earth's core. *Journal of Geophysical Research: Solid Earth, 111*(B6). http://10.1029/2005jb004091

Seto, Y., Nishio-Hamane, D., Nagai, T., & Sata, N. (2010). Development of a software suite on X-ray diffraction experiments. *The Review of High Pressure Science and Technology, 20*(3), 269-276. http://10.4131/jshpreview.20.269

Shahar, A., Schauble, E. A., Caracas, R., Gleason, A. E., Reagan, M. M., Xiao, Y., et al. (2016). Pressure-dependent isotopic composition of iron alloys. *Science, 352*(6285), 580-582. http://10.1126/science.aad9945

Shen, G., Lin, J. F., Fei, Y., Mao, H. K., Hu, M., & Chow, P. (2003). Magnetic and structural transition in Fe_3S at high pressures. *Eos Trans. AGU, 84*(46), F1548-F1549.

Shi, Y.-J., Du, Y.-L., & Chen, G. (2013). First-principles study on the elastic and electronic properties of hexagonal ε-Fe3N. *Computational Materials Science, 67*, 341-345. http://10.1016/j.commatsci.2012.09.012

Sifkovits, M., Smolinski, H., Hellwig, S., & Weber, W. (1999). Interplay of chemical bonding and magnetism in Fe_4N, Fe_3N and zeta-Fe_2N. *Journal of Magnetism and Magnetic Materials, 204*(3), 191-198. http://10.1016/S0304-8853(99)00296-6

Stevenson, D. J. (2001). Mars' core and magnetism. *Nature, 412*(6843), 214-219. http://10.1038/35084155

Takemura, K., & Dewaele, A. (2008). Isothermal equation of state for gold with a He-pressure medium. *Physical Review B, 78*(10). http://10.1103/PhysRevB.78.104119

Thompson, S., Komabayashi, T., Breton, H., Suehiro, S., Glazyrin, K., Pakhomova, A., & Ohishi, Y. (2020). Compression experiments to 126 GPa and 2500 K and thermal equation of state of Fe_3S: Implications for sulphur in the Earth's core. *Earth and Planetary Science Letters, 534*. http://10.1016/j.epsl.2020.116080

Toby, B. H. (2001). EXPGUI, a graphical user interface for GSAS. *Journal of Applied Crystallography, 34*(2), 210-213. http://10.1107/S0021889801002242

Vocadlo, L., Brodholt, J., Dobson, D. P., Knight, K. S., Marshall, W. G., Price, G. D., & Wood, I. G. (2002). The effect of ferromagnetism on the equation of state of Fe_3C studied by first-principles calculations. *Earth and Planetary Science Letters, 203*(1), 567-575. http://10.1016/S0012-821x(02)00839-7

Wetzel, M. H., Schwarz, M. R., & Leineweber, A. (2019). High-pressure high-temperature study of the pressure induced decomposition of the iron nitride γ′-Fe_4N. *Journal of Alloys and Compounds*. http://10.1016/j.jallcom.2019.06.078

Widenmeyer, M., Hansen, T. C., Meissner, E., & Niewa, R. (2014). Formation and decomposition of iron nitrides observed by in situ powder neutron diffraction and thermal analysis. *Zeitschrift fur Anorganische und Allgemeine Chemie, 640*(7), 1265-1274. http://10.1002/zaac.201300676

Wriedt, H., Gokcen, N., & Nafziger, R. (1987). The Fe-N (iron-nitrogen) system. *Bulletin of Alloy Phase Diagrams, 8*(4), 355-377.

Yoder, C. F., Konopliv, A. S., Yuan, D. N., Standish, E. M., & Folkner, W. M. (2003). Fluid core size of Mars from detection of the solar tide. *Science, 300*(5617), 299-303. http://10.1126/science.1079645

Zedgenizov, D. A., & Litasov, K. D. (2017). Looking for “missing” nitrogen in the deep Earth. *American Mineralogist, 102*(9), 1769-1770.

Zhang, W. H., Lv, Z. Q., Shi, Z. P., Sun, S. H., Wang, Z. H., & Fu, W. T. (2012). Electronic, magnetic and elastic properties of ε-phases Fe_3X(X=B, C, N) from density-functional theory calculations. *Journal of Magnetism and Magnetic Materials, 324*(14), 2271-2276. http://10.1016/j.jmmm.2012.02.114

Figure 1.

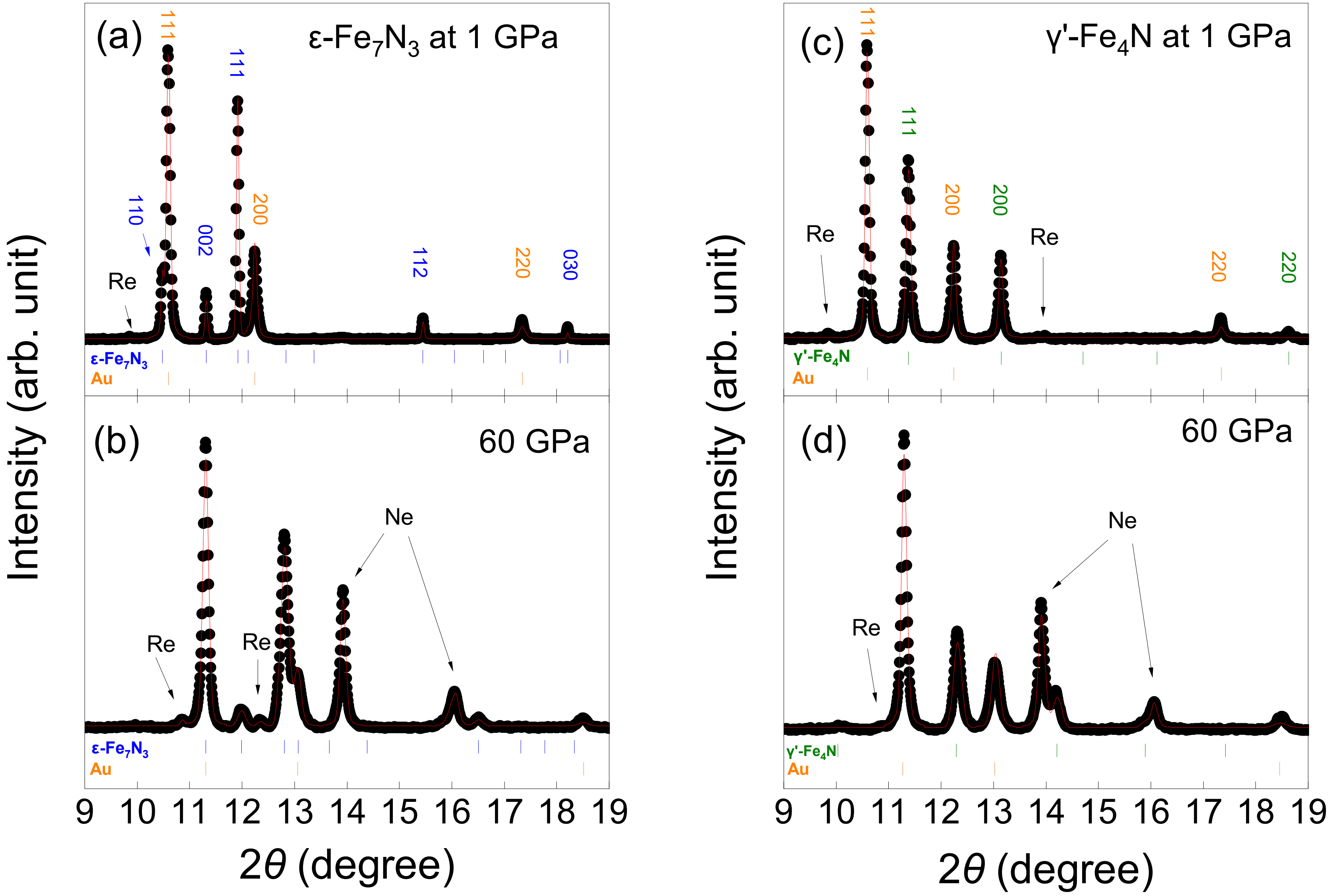

(a)
ε-Fe_7N_3 at 1 GPa
111
110
002
111
200
112
220
030
Re
ε-Fe_7N_3
Au
(b)
60 GPa
Re
Re
Ne
ε-Fe_7N_3
Au
(c)
γ'-Fe_4N at 1 GPa
111
111
200
200
220
220
Re
Re
γ'-Fe_4N
Au
(d)
60 GPa
Re
Ne
γ'-Fe_4N
Au
Intensity (arb. unit)
2θ (degree)
9
10
11
12
13
14
15
16
17
18
19

Figure 2.

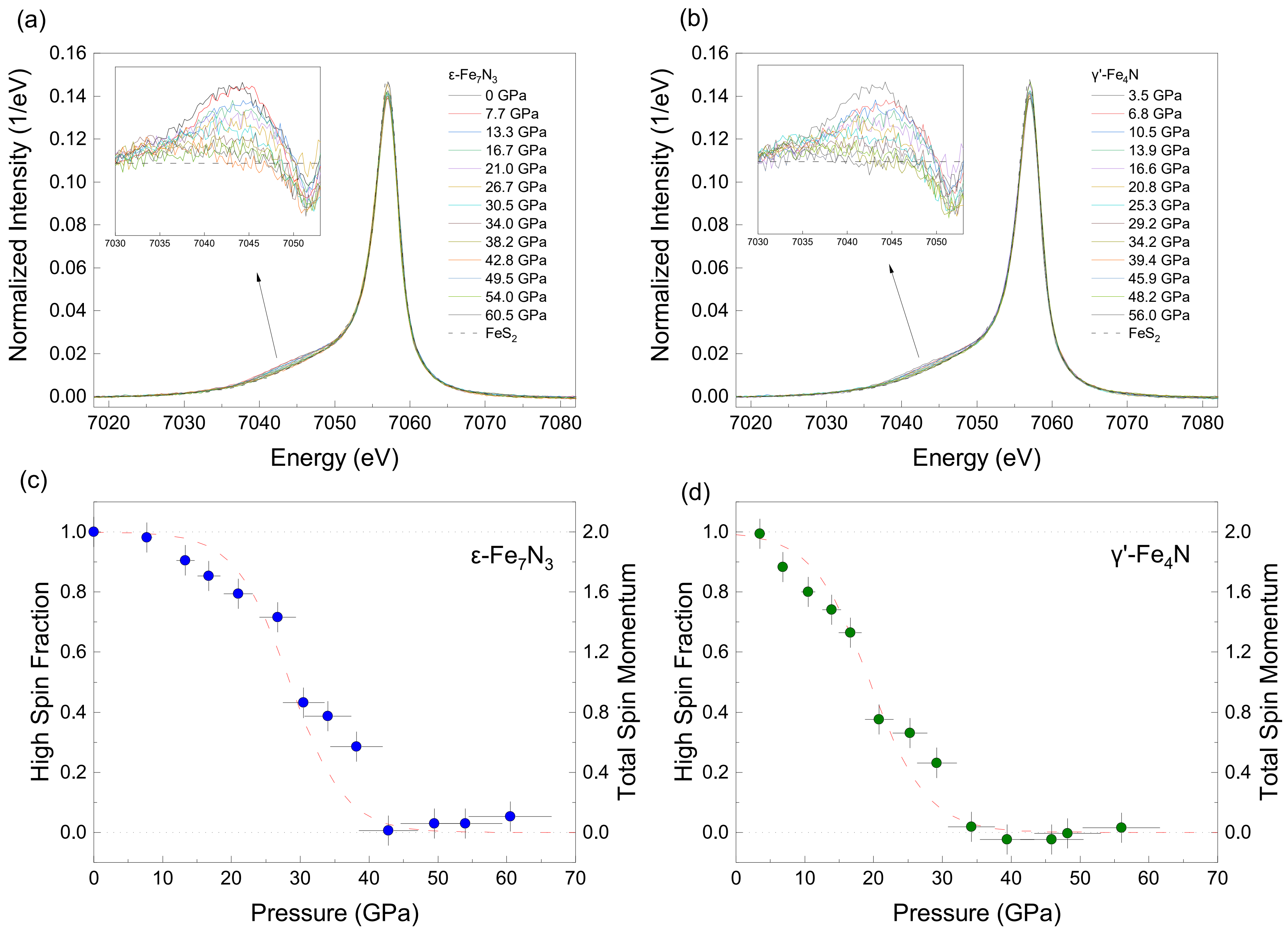

(a)
(b)
(c)
(d)
Normalized Intensity (1/eV)
Energy (eV)
ε-Fe7N3
0 GPa
7.7 GPa
13.3 GPa
16.7 GPa
21.0 GPa
26.7 GPa
30.5 GPa
34.0 GPa
38.2 GPa
42.8 GPa
49.5 GPa
54.0 GPa
60.5 GPa
FeS2
γ'-Fe4N
3.5 GPa
6.8 GPa
10.5 GPa
13.9 GPa
16.6 GPa
20.8 GPa
25.3 GPa
29.2 GPa
34.2 GPa
39.4 GPa
45.9 GPa
48.2 GPa
56.0 GPa
FeS2
High Spin Fraction
Total Spin Momentum
Pressure (GPa)
ε-Fe7N3
γ'-Fe4N

Figure 3.

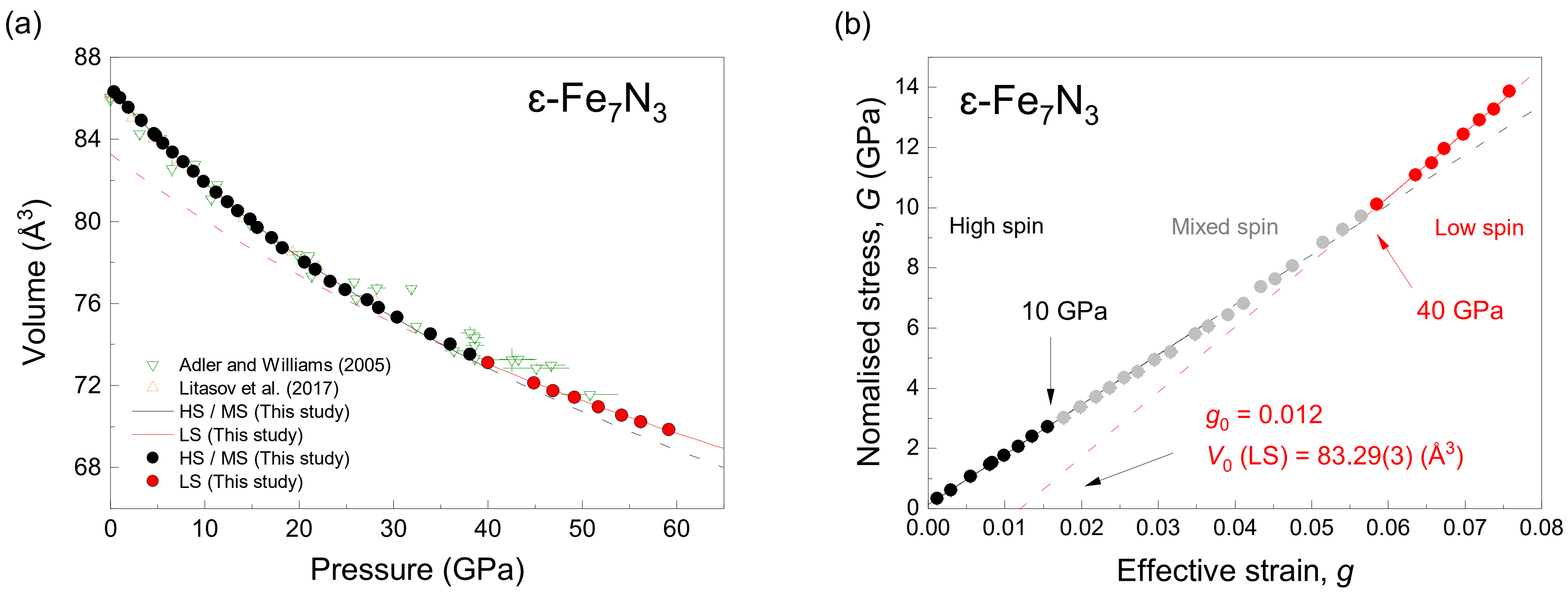

(a)
ε-Fe7N3
Volume (Å3)
Pressure (GPa)
Adler and Williams (2005)
Litasov et al. (2017)
HS / MS (This study)
LS (This study)
HS / MS (This study)
LS (This study)
(b)
ε-Fe7N3
Nomalised stress, G (GPa)
Effective strain, g
High spin
Mixed spin
Low spin
10 GPa
40 GPa
g0 = 0.012
V0 (LS) = 83.29(3) (Å3)

Figure 4.

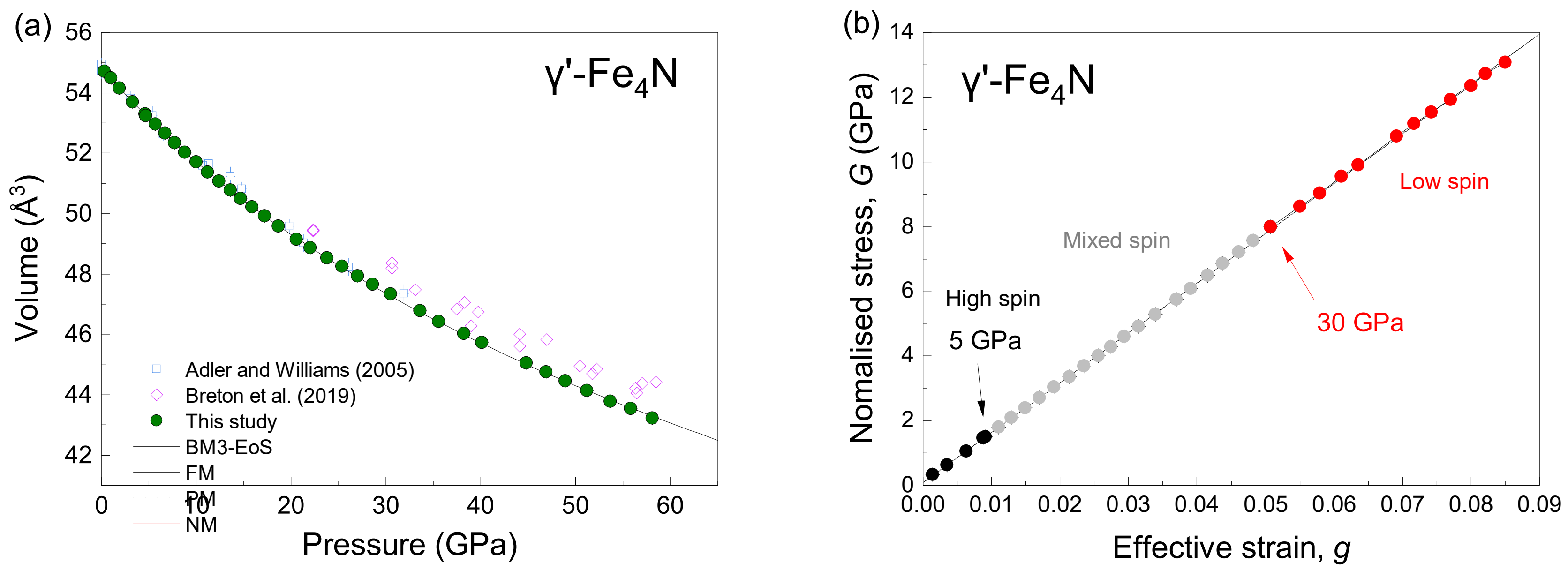

(a)
γ'-Fe_4N
Volume ($Å^3$)
Pressure (GPa)
Adler and Williams (2005)
Breton et al. (2019)
This study
BM3-EoS
FM
PM
NM
(b)
γ'-Fe_4N
Nomalised stress, G (GPa)
Effective strain, g
High spin
5 GPa
Mixed spin
Low spin
30 GPa

Figure 5.

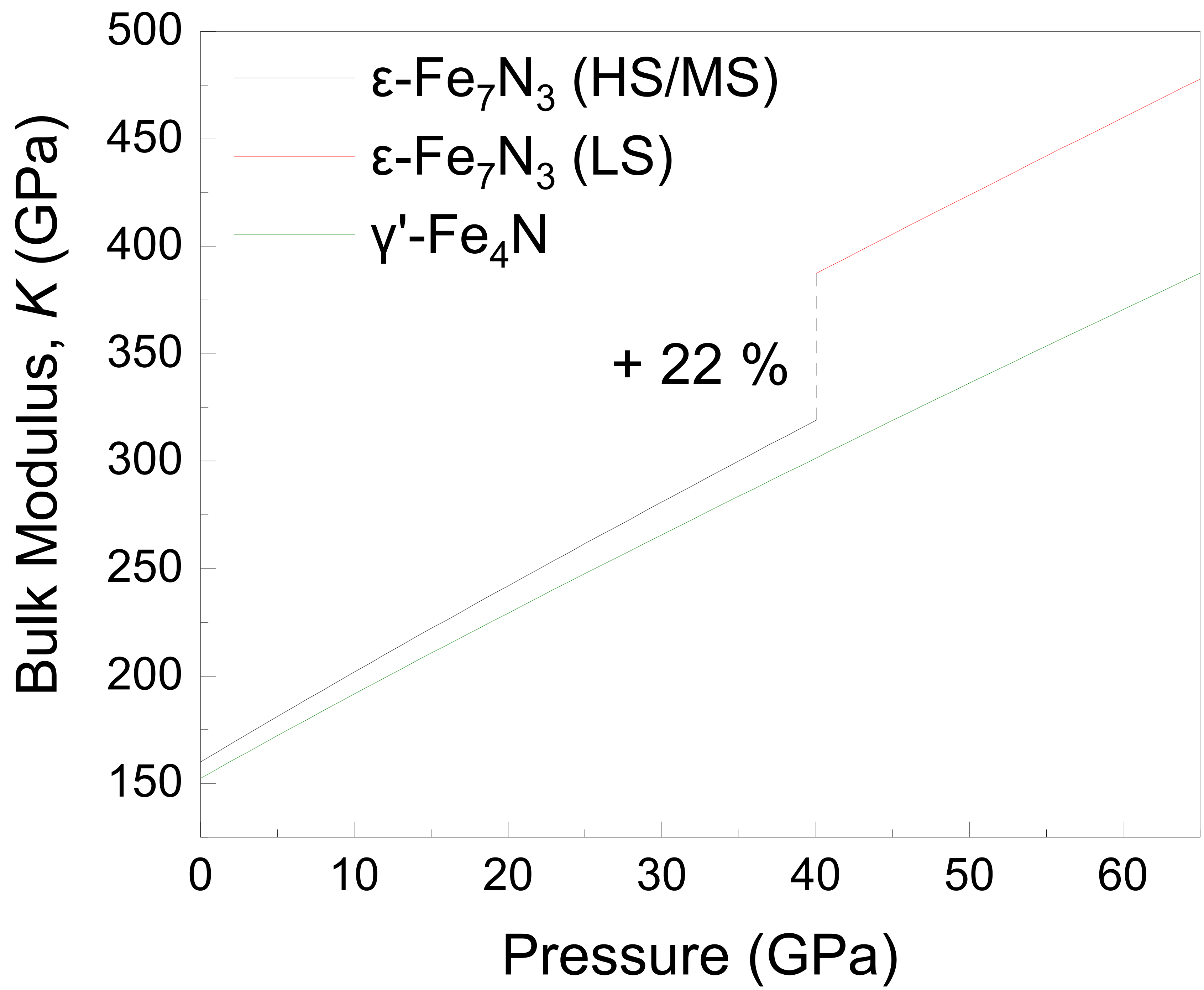

500
450
400
350
300
250
200
150
Bulk Modulus, K (GPa)
ε-Fe7N3 (HS/MS)
ε-Fe7N3 (LS)
γ'-Fe4N
+ 22 %
0
10
20
30
40
50
60
Pressure (GPa)

Figure 6.

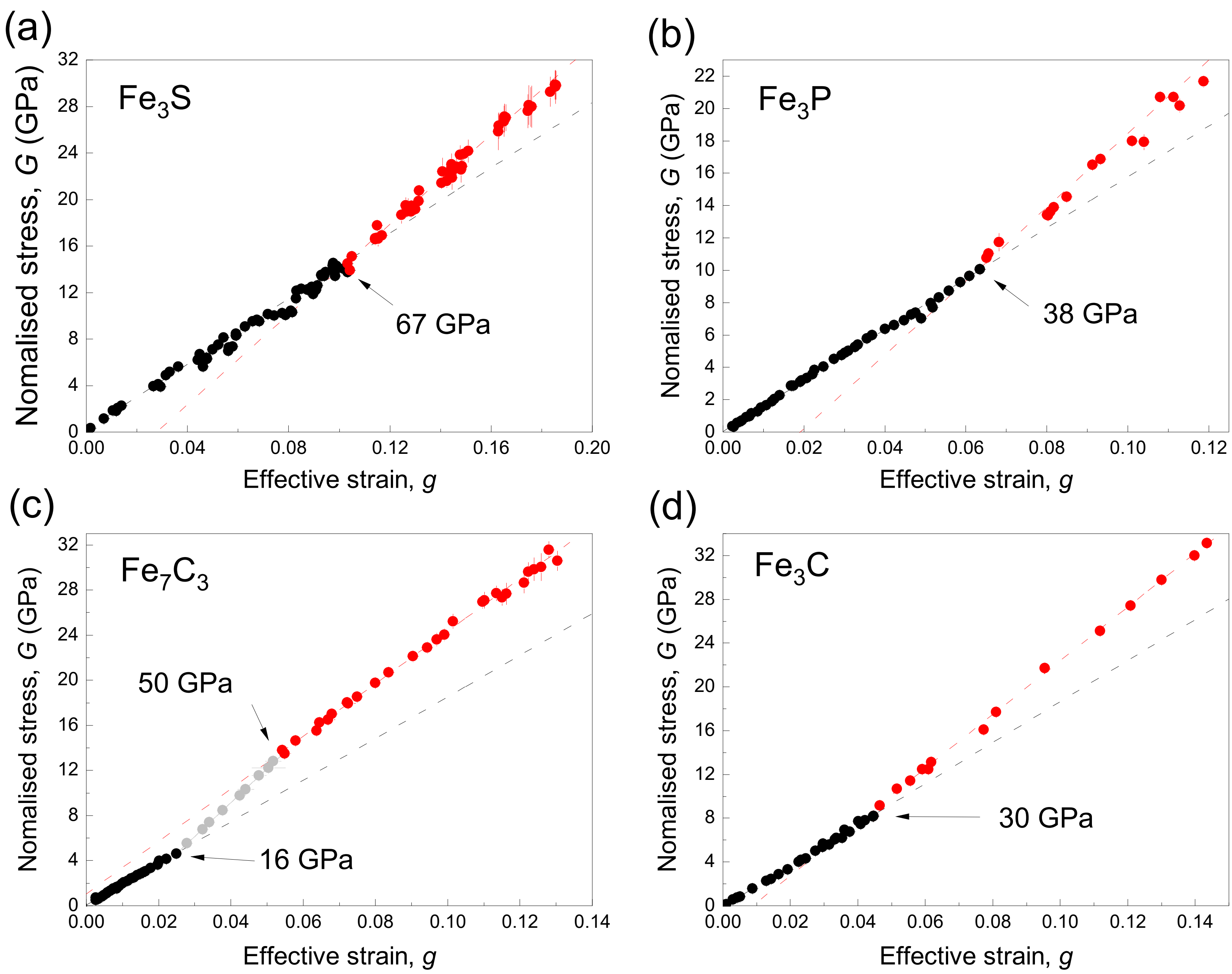
(a)
Fe3S
67 GPa
Nomalised stress, G (GPa)
Effective strain, g
(b)
Fe3P
38 GPa
Nomalised stress, G (GPa)
Effective strain, g
(c)
Fe7C3
50 GPa
16 GPa
Nomalised stress, G (GPa)
Effective strain, g
(d)
Fe3C
30 GPa
Nomalised stress, G (GPa)
Effective strain, g